A Review of High-Speed Aircraft Stability and Control Challenges

Timothy T. Takahashi[1]

Arizona State University, Tempe, AZ, 85281

Jack A. Griffin[2]
Ramana V. Grandhi[3]

Air Force Institute of Technology, Wright Patterson AFB, OH 45433

This paper identifies key stability and control screening parameters needed to design general-purpose high-supersonic and hypersonic aircraft. A review of ground test, computation and flight test data of the rocket propelled Bell X-2, North American X-15, Martin X-24A and Northrop HL-10 lifting bodies, the Lockheed YF-12 (SR-71) and North American XB-70 jet propelled aircraft as well as the Rockwell Space Shuttle Orbiter reveals a need for strong static directional stability. We glean from the relative success of the X-15 and YF-12 and the performance limitations of the others that lateral-directional stability and control needs special scrutiny during preliminary design. We show how adverse yaw can be so strong as to destabilize an otherwise "innocent" looking statically stable airframe like the Bell X-2. This document outlines sources for effective screening criteria that should be considered during high-speed vehicle development. They derive from the classic MIL-STD-8785C, MIL-STD-1797A, MIL-STD-1797B as well as in older AGARD reports.

Select Nomenclature

ALT	= altitude, ft	Izz	= yawing moment of inertia, slug-ft^2
α	= angle-of-attack, º	$LCDP$	= Lateral Control Departure Parameter
b	= span, ft	M	= Mach number
β	= side-slip-angle, º	m	= Mass, slugs
$\bar{c}$	= mean geometric chord, ft	n, n_z	= load factor, -gees
CL	= lift coefficient	p	= roll rate (radian/sec)
$dCl/dail$	= roll moment coefficient due to aileron, 1/º	q	= pitch rate (radian/sec)
$dCl/d\beta$	= roll moment coefficient due to sideslip, 1/º	r	= yaw rate (radian/sec)
Clr	= roll damping due to yaw rate	$\bar{q}$	= dynamic pressure, lbf/ft^2
Cnr	= yaw damping due to yaw rate	S_{ref}	= reference area, ft^2
$dCm/d\alpha$	= pitch moment coefficient due to α, 1/º	t	= time, sec
Cmq	= pitch damping due to pitch rate	W	= weight, lbm
$dCn/dail$	= yaw moment coefficient due to aileron, 1/º	ω_{sp}	= Short-Period freq, Hz or-radian/sec
$dCn/d\beta$	= yaw moment coefficient due to sideslip	ω_{dr}	= Dutch-Roll freq, Hz or-radian/sec
Cnp	= yaw damping due to roll rate	ζ_{sp}	= Short-Period Damping Ratio
Clp	= roll damping due to roll rate	ζ_{dr}	= Dutch-Roll Damping Ratio
$delev$	= elevator deflection, º	τ_s	= Spiral-Mode Time Constant, sec
ϕ	= bank angle, º	τ_r	= Roll-Mode Time Constant, sec
Ixx	= rolling moment of inertia, slug-ft^2	$VKTAS$	= Velocity in true airspeed, nM/hr
Iyy	= pitching moment of inertia, slug-ft^2		

---

[1] Professor of Practice – Aerospace Engineering, School for the Engineering of Matter, Transport and Energy. AIAA Associate Fellow.
[2] Research Engineer. AIAA Member.
[3] Professor, Department of Aeronautics and Astronautics. AIAA Fellow.

I. Introduction

HYPERSONIC aircraft, those that fly at least five times the speed of sound, present a challenging design problem. In order to cover great ground distances in a brief moment of time, such as New York to Tokyo in less than two hours or a 500-NM stand-off military mission within 10 minutes, a successful design must demonstrate positive stability and broad capabilities for controllability across wide speed / altitude envelope. The Rockwell Space Shuttle Orbiter [1] and the North American X-15 rocket plane [2][3] are two successful general-purpose hypersonic aircraft that employed different strategies to ensure positive controllability. This review of screening methods suitable for preliminary design studies helps reduce stability and control development risk for future high-speed aircraft.

The challenge thus presented can be summed up neatly by a quip made by author Takahashi's mentor (now deceased) Professor Emeritus W.H. Mason. He noted that during conceptual and preliminary design "the Flight Control Guys, if they're even there, [say] 'We need a complete aero math model from -90° to +90° or else forget it.' [Whereas] the Conceptual Design Guys say, 'just use the usual tail volume coefficient.'" [4] Takahashi's personal experience, having worked on industrial hypersonic development programs, is that neither approach promotes rapid convergence to a successful configuration; this is because "everything affects everything" especially at high Mach numbers.

Because our review of prior literature (including Ref. [4]) revealed that most existing treatises discuss aerodynamic stability and control from an analytical detail design perspective, we feel that a modern survey paper considering proactive conceptual design screening methods is in order. As such, we follow in the footsteps of Coleman & Faruqi [5], Larson, et al [6] and Day [7].

In this work, we document a number of parameters, many first identified to support maneuvering fighter aircraft design. They serve as powerful discriminators to separate low-risk from high-risk aerodynamics. We recommend applying these screening methods to evaluate candidate configurations for future programs; their use may reveal severe operational envelope restrictions which would compromise otherwise promising designs.

Fig. 1 The AIM-9X "Sidewinder" represents a long-lived sucessful family of high-speed "traditional" missiles. [8]

Fig. 2 The North American X-15. History's most successful general-purpose powered hypersonic aircraft. [3]

II. High-Speed Vehicle Design Philosophy

Fundamentally, aircraft need to be controllable to be able to fly where they are commanded to go. They do this by climbing and descending, accelerating and decelerating and by changing course heading.

Hypersonic flight vehicle design may be approached from the viewpoint of: 1) nearly-axisymmetric missile design (skid-to-turn), 2) traditional aircraft design (bank-to-turn) or 3) a hybrid containing elements of both. The AIM-9 "Sidewinder" represents an early successful air-to-air weapon capable of flight at $M > 2$. [8] It features the classic configuration: solid-rocket motor propelled cylindrical body festooned with moveable, cruciform fins; see Fig. 1. Later variants employ thrust-vectoring of the solid rocket motor to enhance maneuvering control. Conversely, the rocket propelled North American X-15 is a slender, conventional aircraft with a fuselage, wings and clearly differentiated horizontal and vertical stabilizers; see Fig. 2. [3] The much more recent Boeing X-51A represents a hybrid approach to configuration: at launch, a thrust-vector-controlled MGM-140 solid-rocket booster accelerates it to cruise conditions; at hypersonic cruise, it is flown as a liquid-fueled scramjet powered aircraft featuring four tail fins; see Fig. 3. [9]
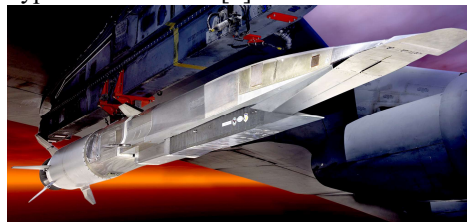

Fig. 3 The Boeing X-51 Hypersonic Scramjet Demonstrator shown mated to the MGM-140 ATACMS solid rocket booster. [9]

Traditional missile Guidance, Navigation and Control (GN&C) strategies employ a "skid-to-turn" maneuvering philosophy. Under this paradigm, the airframe does not roll to any particular preferred angle; instead, the GN&C system commands the control surfaces to directly maneuver in the desired direction. A skid-to-turn missile will fly over a wide range of angle-of-attack (α) as well as sideslip angles (β).

Traditional aircraft GN&C strategies employ a "bank-to-turn" maneuvering philosophy. Under this strategy, the airframe has a clear "top" and "bottom;" the controller will that the "top" is always the "leeward side" and the "bottom" is always the "windward side." To turn, the GN&C system will direct the aircraft to roll to a preferred bank angle (ϕ) so that centripetal accelerations can change course heading. While a bank-to-turn aircraft may fly over a wide range of angle-of-attack, they will always be constrained to fly at minimal sideslip.

Depending upon its intended use, hypersonic aircraft may operate far from traditional "lift-equals-weight" ($n_z \sim 1$) flight. Many X-15 trajectories (see Fig. 4) took the aircraft to such altitudes that despite its hypersonic speed, dynamic pressure dropped far below its "1-gee stall speed." [10] "Over-the-top," the X-15's aerodynamic control diminishes to the point where it needs reaction control jets (RCS) for attitude, sideslip and roll control. [10] Upon reentry, the X-15 flew at relatively high angles-of-attack. Around 180,000-ft the pilot would use the RCS to establish a target angle-of-attack. As the aircraft flew deeper into the atmosphere, the normal forces would build from near zero (a ballistic trajectory) to peak above 4-gees around 80,000-ft. In prior work, Griffin & Takahashi [12] found that X-15 if flown wings-level, could not perform an aerodynamic braking maneuver; the wings would provide enough lift to have the airframe "skip" back out of the atmosphere rather than reenter. Consequently, the X-15 flew much of its lifting reentry in a steep bank ($\phi \sim 75°$).

For similar reasons, the Space Shuttle Orbiter flies its reentry at steep bank angles; see Fig. 5. [11] Not only does this mitigate against atmospheric "skip," but by scheduling the symmetry (or asymmetry) of the banked roll maneuvers, the Orbiter can steer towards a cross-range landing point. Note that it flies atmospheric entry at $\phi > 60°$; the first time that it glides wings level for any period of time is during final approach and landing where $M < 1.5$ and $ALT < 60,000$-ft.
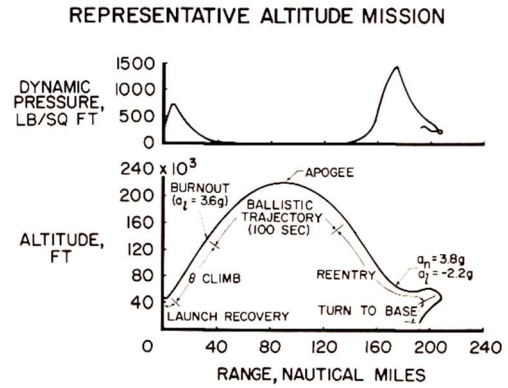

Fig. 4 X-15 High Altitude Mission Trajectory showing the wide range of dynamic pressure encountered as well as the 3.8-gee load factor developed during lifting reentry. [10]
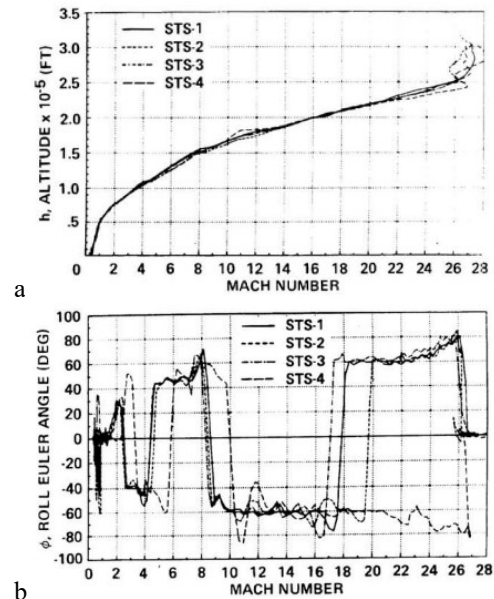

a

b

Fig. 5 Space Shuttle Orbiter Reentry Trajectory [11]

For the purposes of this paper, we will consider necessary stability and control screening methods to support the development of a general purpose "bank-to-turn" hypersonic aircraft. These methods are general enough to encompass flight at low ($\bar{q} <= 35$-lbf/ft²), medium (35-lbf/ft² $< \bar{q} < \sim 500$-lbf/ft²) and high dynamic pressures ($\bar{q} > 500$-lbf/ft²) both as a powered aircraft and as a glider. These methods should be suitable to support design studies for diverse vehicles including reusable orbital spacecraft, hypersonic boost-glide as well as hypersonic cruise vehicles.

Approved for Public Release – Case Number: 2022-0708

III. Basics of High-Speed "Hypersonic" Aerodynamics

"Hypersonic flight" describes operations under a broad tent of speeds, flow physics and atmospheric properties. Colloquially, the hypersonic flight regime begins when a vehicle operates at freestream $M > 5$. More practically, hypersonic flight occurs at speeds where simple sweep theory and slender body theory no longer applies; in other words, flight at conditions where the Mach cone is so swept that all shapes have "supersonic leading edges" including the fuselage.
+
Hypersonic flight conditions also occur at speeds where localized aerodynamic heating is important. If flow field temperatures substantially rise above freestream, the local flow velocity is no longer linearly proportional to its Mach number; this is because the speed of sound in a fluid is proportional to the square root of its absolute temperature. As the momentum / Mach number relationship falls apart, an entropy / enthalpy viewpoint is needed to model fluid flows since most of the total temperature inherent in the flow exists as kinetic energy. If the local flow gets hot enough, diatomic elements in air (O_2 and N_2) disassociate. Not only is there a latent heat of dissociation to consider, but the specific heat ratio of dissociated free-molecular oxygen and nitrogen is no longer $\gamma \sim 1.4$. During early reentry, where the atmosphere is highly rarified, the continuum model of fluid flow may no longer apply.

What is most important from the point of hypersonic vehicle stability and control derives from the physical definition of the pressure coefficient: $Cp = \frac{(p - p_\infty)}{(p_0 - p_\infty)}$; where p is the local pressure, p_∞ is the static pressure in the freestream and p_0 is the stagnation pressure in the freestream. We can see from this relationship that as the Mach number increases, so does the stagnation pressure, leading to the trend that the Cp which represents a perfect vacuum (the physical limit to pressure) becomes a strong function of freestream Mach number and trends to zero as the Mach number approaches ∞. $Cp_{vac} = -\frac{1.43}{M^2}$; see TABLE 1. [13]

To illustrate the significance of the vaccum condition, consider the pressure profiles over a NACA 0012 airfoil at incompressible speeds; Fig. 6. [14] At low speed, the majority of the lift is developed from underpressures ($Cp < 0$) on the leeward side of the airfoil. For this example, we can see that stagnation ($Cp \sim 1$) forms on the windward side, while the peak under pressure ($Cp \sim -5$) occurs near the leading edge on the leeward side. As the freestream Mach number increases past $M = 0.5$, we see that $Cp \sim -5$ represents a physically impossible pressure; a pressure less than a pure vacuum. This highlights two trends of hypersonic aerodynamic flows: 1. that the source of lift gradually changes from being leeward surface geometry driven (at subsonic speeds) to being entirely windward surface geometry driven (at hypersonic speeds) (see Fig. 7) and 2. that

TABLE 1 Minimum Cp limits due to vacuum as a function of freestream Mach number.

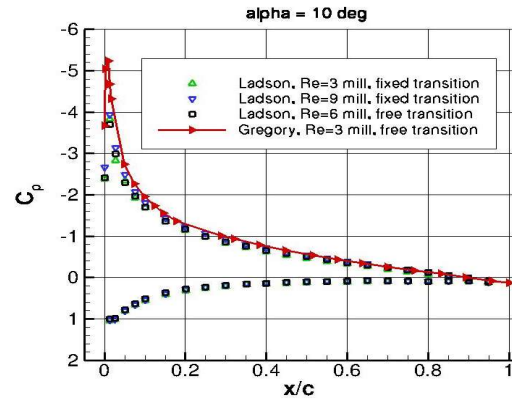| Mach	Cp Vacuum	Cp 70% Vacuum
0.1	-143.	-100.
0.5	-5.72	-4.00
0.8	-2.23	-1.56
0.9	-1.76	-1.24
1	-1.43	-1.00
1.2	-0.993	-0.695
1.6	-0.559	-0.391
2	-0.358	-0.250
3	-0.159	-0.111
4	-0.089	-0.063
5	-0.057	-0.040
6	-0.040	-0.028
7	-0.029	-0.020
8	-0.022	-0.016
10	-0.014	-0.010

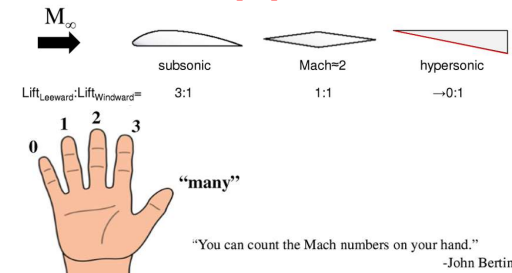Fig. 6 Low-Speed Pressure Coefficients over a NACA 0012 airfoil. [14]

Fig. 7 – Mach number dependent trends in the windward side dominance of aerodynamic forces [15]

at hypersonic speeds, localized chemistry and enthalpy on the windward surfaces dominate rather than generalized freestream Mach number effects. [15]

This trend manifests itself in the Mach number dependence of $dCL/d\alpha$, see Fig. 8. [16] As flight speeds increase from the incompressible through the transonic, $dCL/d\alpha$ first increases (following the Prandtl-Glauert rule). At supersonic speeds, $dCL/d\alpha$ begins a long decrease, following the Ackeret rule. The decline in $dCL/d\alpha$ stems largely from the reduction and eventual loss of leeward side lift generating capability. Consequently, as freestream Mach number increases, an aircraft will have to trim at ever increasing α to maintain a constant CL.

A further byproduct of this trend manifests itself in the change in the slope of $dCn/d\beta$. In order to provide directional stability, aircraft have vertical projected area aft of their center-of-gravity (CG). Since the vertical tail needs to provide restoring moments against yaw disturbances rotating the aircraft to both the left and right, the default configuration for vertical tails is a thin, symmetric surface. As the Mach number increases, the loss of the ability of the leeward side to develop suction manifests itself as a decline in directional stability; it can no longer promote stable flight. If we turn to Fig. 9, we can see the design solution chosen by the North American X-15 engineers. While the wing and horizontal tails are thin, the vertical fin is a thick 10° included angle wedge. [3] From a nose on perspective, with the fin aligned with the body, it presents two windward sides (port and starboard) at all angles-of-attack provided the sideslip-angle remains small (-5° < β < +5°). [17] This design feature largely mitigates any further losses in directional stability at $M > 2$ (where a thin airfoil would have a 50/50% balance in forces developed by the windward and leeward surfaces).

Fig. 8 $dCL/d\alpha$-vs-Mach of the North American X-15. [16]

We will show later in this paper, how the thick wedge tail was essential to establishing the favorable general flying qualities of the X-15.

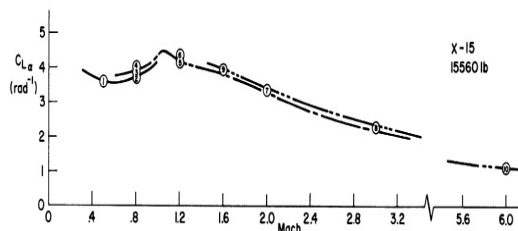## IV. Flight Dynamics Issues Pertinent to High Speed Flight

Fundamentally, aircraft have six degrees of freedom in motion: Translations in the *x, y* and *z* coordinate frame (either body aligned, earth aligned, or flight path aligned) and rotations about the *x, y* and *z* axes (roll, pitch and yaw); see Fig. 10.

To gain an understanding of the "art-of-the-possible" with configuration aerodynamics, remember the impact of geometry on these forces and moments. Lift is the aggregate contribution of all surface pressures in the vertical direction (orthogonal to the on-coming wind). Drag is the aggregate contribution of all surface pressures and traction aligned with the on-coming wind. Side force is the aggregate contribution of all surface pressures orthogonal to lift and drag.

Pitching moment arises from the longitudinal distribution of lifting elements relative to the center of gravity location. Similarly, rolling and yawing moment arises from the lateral and longitudinal distribution of side force generating

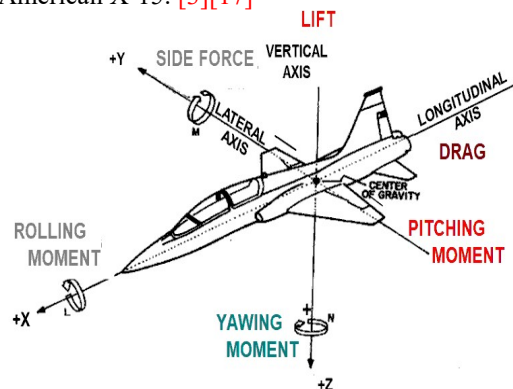Fig. 9 10° Wedge Vertical Tail on the North American X-15. [3][17]

Fig. 10 Force & Moment Axis System for Aerodynamics. Traditional stability axis has Lift & Drag aligned with the oncoming wind, Side Force and Moments aligend with the body.

5

elements. Because the actual center-of-gravity (*CG*). location may shift with changing payload and fuel loads, we aerodynamicists typically compute aerodynamic forces and moments about a nominal *CG* location, this position is known as the moment reference point (*MRP*). On an actual mission, the *CG* position may move around with changing payload and fuel loads, and as such any rapid stability screening method must address *CG* travel over the course of a flight. [18]

Larson, et al [6] noted that hypersonic vehicles exhibit "unconventional, configuration-dependent dynamic issues that impact … flying qualities." They are "associated with configuration features set by propulsion and/or aerodynamic performance considerations essential to achieve hypersonic flight." [6] Consequently, "these characteristics are "unalterable" even though they may be directly or indirectly adverse from the standpoint of flight control and flying qualities." [6] They note that high-speed / high-attitude aircraft may exhibit novel dynamic modes which are not seen on slower aircraft. They also note that high-speed vehicles may be prone to both open-loop as well as closed-loop instabilities which place additional demands on the control system; especially since high-speed vehicles are likely to have "structural modes which are sufficiently low in frequency to have significant interactions with the high bandwidth controllers involved in stability augmentation functions." [6]

In this section, we will discuss the basic equations needed to specify and evaluate 1) control authority, 2) aircraft stability and 3) aircraft maneuvering control response to attain mission goals.

A. Trimmed Aerodynamics

In theory, when all forces and moments are in perfect equipoise the aircraft will fly straight and level. This represents a perfect trimmed condition, where Lift = Weight, Thrust = Drag and Side Force = 0.

The first goal of a control authority specification is to demonstrate aircraft trim with reasonable control surface deflections across the entire flight envelope, that is a combination of weight, *CG* position, flight speed (*M*), altitude (*ALT*) and attitude (*α* and *β*). A typical requirement might require the preliminary design team to establish basic static trim using no more than 75% of the maximum, theoretical control power. [19][20] Control power must also be sufficient to command pitching, rolling and yawing maneuvers, to suppress oscillatory modes and possibly to augment inherent aerodynamic stability.

In reality, the concept of perfectly steady straight-and-level flight is a mirage. Aircraft tend to exhibit residual oscillations following their inherent Rigid-Body modes. In pitch, the more-or-less rapid porpoise-like mode where the angle-of-attack varies with minimal impact to airspeed or altitude is known as the Short-Period mode. The "effective spring constant" in this mode is controlled by the change in pitching moment with respect to angle-of-attack, the dynamic pressure and the basic size of the aircraft; see Fig. 11.

Because aircraft have inherent bilateral symmetry, one would think that lateral and directional trim problems would be simple to solve; this is not so because aircraft have no inherent pendulum stability. In order for aircraft to remain

Fig. 11 Short-period Rigid-Body Mode Schematic

"top-side-up" they need to be being locked into a stable oscillatory mode with synchronized motions in both yaw and roll – this is known as the Dutch-Roll mode.
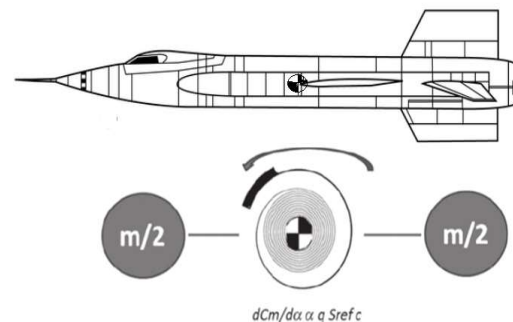
Depending upon the basic configuration, the inherent fixed control surface stability and control characteristics of the airplane may not be satisfactory. Over the next few subsections, we will show how the rigid-body behavior may prove troubling, including a trend to insufficient damping which leads to "wallowing" or "porpoising" flight and/or difficulties holding bank angles (and as such, maintaining heading change). Some of these deficiencies may be corrected through the use of a command augmentation system (*CAS*) or a stability augmentation system (*SAS*). At noted by Larson [6], many of these congenital issues prove unsolvable; the "computer," even when programmed with sophisticated feedback control algorithms, cannot always rectify certain stability problems inherent with hypersonic aerodynamics.

Approved for Public Release - Case Number: 2022-0708

B. Approximate Longitudinal Dynamics

A typical performance specification for flying qualities defines desired boundaries in terms of speed and altitude for both steady, level flight ($n_z = 1$) as well as maneuvering flight ($n_z \neq 1$, climb/descend, accelerate/decelerate, and roll into and out of banked turns).

Traditionally aerodynamicists define the static margin as a measure of an air vehicle's longitudinal stability. The pitching moment represents the torque developed by the center-of-lift (often called the center-of-pressure, CP) acting upon a lever-arm whose length represents the distance from the CP to the moment-reference-point, MRP. In traditional aircraft nomenclature, these positions are given in terms of fuselage station values which grow more positive as one moves aft on the physical vehicle. If the CP is aft of the CG, the aerodynamics will develop a nose-down pitching moment. If the CP is ahead of the CG, the aerodynamics will develop a nose-up pitching moment. In our convention, the pitching moment coefficient may be written as:

$$Cm = \frac{LIFT(CP-CG)}{\bar{q}\,Sref\,\bar{c}} \tag{1}$$

The static margin represents a somewhat different value, that is the implied distance from the aerodynamic-center (AC), the virtual location where pitching moment torques are invariant to small changes in angle-of-attack, to the MRP. If the aerodynamic-center is aft of the CG, the vehicle will develop an increasing nose-down torque in the presence of any nose-up perturbations to flight. If the aerodynamic-center is ahead of the CG, the vehicle will develop destabilizing nose-up torques in the presence of any nose-up perturbations to flight.

Because the CP represents the centroid of all lifting forces acting upon an airframe, it is dependent upon the angle-of-attack (α), speed (M) and control surface deflections. Thus, to place an aircraft in pitch trim (where pitching moments are neutralized) requires control surfaces to be deflected to make the CP longitudinally coincident with the CG.

While pitch trim is an essential component of steady level flight, it is not the only criteria. The equilibrium trim point needs to be stable, in that the response to perturbations should restore equilibrium; see Fig. 12. To achieve inherent static stability, the AC must be placed behind the CG for all operating conditions. For most low-speed aircraft, the AC position is a function of Mach number and angle-of-attack but does not change appreciably as the control surfaces deflect. At hypersonic speeds, the AC couples noticeably with the deflection of primary pitch control surfaces further complicating analysis.

Fig. 12 Distinction between trim and stability

The inherent Short-Period rigid-body oscillatory mode of the aircraft (frequency in radian/sec) at a given speed (M) and angle-of-attack (α) may be approximated, using the physical analogy shown in Fig. 11, as:

$$\omega_{SP} \approx \sqrt{\frac{-5\ .3\frac{dCm}{d\alpha}\bar{q}\,Sref\,\bar{c}}{Iyy}} \tag{2}$$

Where $dCm/d\alpha$ is given in terms of customary units, per degree. [18][21][22][23]

For an aircraft with irreversible control surfaces lacking a feedback control system to alter the short-period frequency, the value $dCm/d\alpha$ represents the inherent vehicle aerodynamic properties with the control surfaces deflected to attain pitch trim ($Cm = 0$). To further complicate matters, aircraft may be fitted with a feedback control system that synthesizes an "apparent" static stability with the "stick fixed" even if the aircraft is fundamentally unstable (i.e., $dCm/d\alpha > 0$) in the absence of the feedback control system. By deflecting aerodynamic surfaces proportional to sensed deviations from the desired trimmed angle-of-attack, the control system will synthesize an apparent $dCm/d\alpha$ which will define the "closed loop" Rigid-Body mode natural frequency.
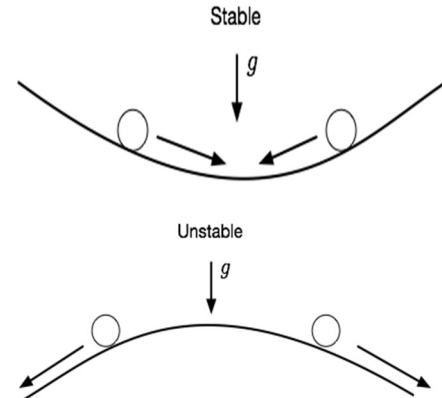
Approved for Public Release - Case Number: 2022-0708

Similarly, the short-period damping ratio may be estimated as:

$$\zeta_{SP} \approx -\frac{M_q + Z_a/U_1}{2\,\omega_{SP}} \tag{3}$$

Where

$$M_q = \frac{Cm_q\,\bar{q}\,Sref\,\bar{c}^2}{2\,Iyy\,VKTAS\left(\frac{6076}{3600}\right)} \tag{4}$$

and

$$\frac{Z_a}{U_1} \approx -\frac{\bar{q}\,Sref}{m\,VKTAS\left(\frac{6076}{3600}\right)}\left(57.3\frac{dCL}{d\alpha}\right) \tag{5}$$

Cm_q represents the variation in pitching moment coefficient with pitching rate in radian/sec. For an aircraft with irreversible control surfaces lacking a feedback control system to alter the short-period damping, the value of Cm_q represents the inherent vehicle aerodynamic properties. [21][22][23] As with other fundamental properties, Cm_q is a function of Mach number; it tends to decline with increasing Mach number as vehicle aerodynamics becomes increasingly windward surface dominated.

The presence of the true airspeed in the denominator of both terms controlling the damping ratio is important for hypersonic flight because the damping ratio (holding short-period frequency constant) declines inversely proportional to *VKTAS* given constant Cm_q and $dCL/d\alpha$. In reality, since both Cm_q and $dCL/d\alpha$ tend to decline with increasing Mach number, the loss of damping is more severe yet; see Fig. 13. Absent any sort of synthetic stability system, as airspeed increases from 200-KTAS to 4,000-KTAS (i.e., $M = 0.3 \rightarrow \sim 6$), the damping factor will decline by a factor of at least 20. See Fig. 14 to contrast the time history of a system with $\zeta \sim 0.5$ to $\zeta \sim 0.025$. An aircraft with inherent short-period pitch damping of $\zeta \sim 0.5$ would be easy to fly; one with $\zeta \sim 0.025$ will be so lightly damped as to be nearly impossible to control absent some form of artificial pitch damping.

Fig. 13 Mach number effects on Pitch Damping coefficient (Cm_q) North American X-15. [16]

Fig. 14 Example of loss of short-period damping ratio associated with hypersonic flight.

This "feature" of the equations of motion means that even statically stable hypersonic airframes, which develop otherwise favorable stick-fixed short-period frequencies, need closed-loop feedback augmentation in order to provide a level of damping needed to successfully perform their intended mission. Thus means that a purely static stability analysis is unreliable to screen a design; acceptable hypersonic stability requires an active control system that is robust enough to account for uncertainties in the predicted and/or computed aerodynamic design parameters and "real world" atmospheric disturbances. Depending upon available control power, such as system may prove impossible to implement.

Rudd, et al [24] noted that when comparing dynamic models of the XB-70, the X-15 and a generic hypersonic "caret" waverider that one can neglect the dynamic derivatives (i.e. assume that they are all zero) when analyzing such configurations at speeds above Mach 3.0. We concur that the inertial terms (those inversely proportional to true airspeed) in the damping equations (refer back to Eq. (3), (4) and (5)) overwhelm probable aerodynamic damping at very high Mach numbers.

We must also consider a second longitudinal oscillatory mode, the Phugoid; where kinetic energy (i.e., airspeed) and gravitational potential energy (i.e., altitude) freely exchange with one another. [21][22][23] This represents a surging motion where a gain in altitude is associated with a loss of airspeed; lost altitude is similarly associated with a gain in airspeed. Since kinetic energy of an aircraft greatly exceeds its potential energy due to altitude at hypersonic speeds; lightly damped Phugoidal modes may traverse a wide variation in altitude. [25]
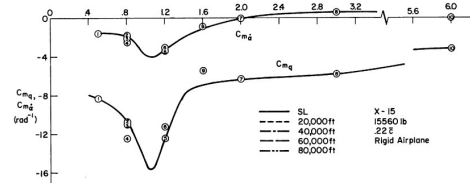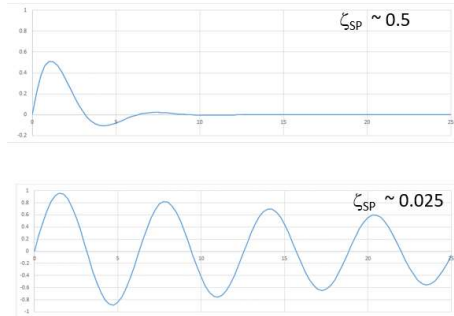
The Phugoid natural frequency (in radians per second) may be approximated by:

$$\omega_{PH} \approx \sqrt{2} \frac{32.2}{VKTAS \left(\frac{3600}{6076}\right)} = \frac{76.85}{VKTAS} \tag{6}$$

And the consequent damping ratio as:

$$\zeta_{PH} \approx \frac{0.707}{L/D} \tag{7}$$

Once again, note the presence of the true airspeed in the denominator of Phugoid frequency equation. The faster we fly, the slower the Rigid-Body mode becomes. At 200-KTAS, the Phugoid frequency is ~0.38-radian/sec (i.e., a period of ~16-sec); at 4,000-KTAS, the Phugoid frequency is ~0.02-radian/sec (i.e., a period exceeding 5-min). Because hypersonic airframes are not known for their high aerodynamic L/D, we see that Phugoid damping is also unlikely to pose a problem. At $L/D \sim 1$, $\zeta_{PH} \sim 0.7$ (very well damped); at $L/D \sim 3$, $\zeta_{PH} \sim 0.23$.

C. Approximate Dutch-Roll Lateral-Directional Dynamics

Since aircraft have no inherent pendulum stability, they remain "top side up" only when they display stable oscillatory Dutch-Roll motions. They also may display stable or unstable non-oscillatory behaviors in pure Direction, Roll and in Spiral flight path.

Directional-Divergence is the byproduct of a statically unstable airplane in yaw. In the absence of a stable Dutch-Roll Mode arising from a strong dihedral effect ($dCl/d\beta < 0$) occurring at high angles of attack $sin(\alpha) >> 0$, a yaw perturbation will result in a continuing yaw out of the wind if $dCn/d\beta < 0$, i.e., a spin. [21][22][23]

Next, we present the Dutch-Roll mode. The Dutch-Roll mode is typically a lightly damped oscillatory mode coupling roll and yaw motions. [18][21][22][23][26] If a statically stable aircraft encounters an initial disturbance that gives it a positive sideslip angle ($\beta > 0$) (i.e., a leftward disturbance), the aerodynamic rolling ($dCl/d\beta < 0$) and yawing ($dCn/d\beta$) moments due to sideslip will cause the right wing to rise and the nose will swing to the right. Oscillations will continue until aerodynamic damping cause the motion to die away.

The Dutch-Roll frequency in radian/sec may be estimated by:

$$\omega_{DR} \approx \sqrt{\frac{57.3 \, C_{n\beta dynamic} \, \bar{q} \, Sref \, b}{I_{zz}}} \tag{8}$$

Where $C_{n\beta dynamic} = \frac{dCn}{d\beta} cos(\alpha) - \frac{dCl}{d\beta} sin(\alpha) \left(\frac{Izz}{Ixx}\right)$. If $C_{n\beta dynamic}$ goes negative, the aircraft will not oscillate, instead will depart. We can see that $C_{n\beta dynamic}$ is dominated by the static weathercock stability ($dCn/d\beta$); the larger the vertical tail, the more positive $C_{n\beta dynamic}$. As the angle-of-attack increases, the dihedral effect plays an additional stabilizing role ($dCl/d\beta < 0$ and $Izz/Ixx >> 1$ for slender, swept configurations). [18][21][22][23][26] In AGARD CP-235 Skow recommends that $C_{n\beta dynamic} > +0.004$ to ensure adequate stability to prevent yaw departures regardless of the implied Dutch-Roll frequency. [27]

Similarly, the Dutch-Roll damping ratio may be approximated by: [21][22][23]

$$\zeta_{DR} \approx -\frac{(N_r + \frac{Y_\beta}{U})}{2 \, \omega_{DR}} \tag{9}$$

where

$$\frac{Y_\beta}{U} = 57.3 \frac{dCY}{d\beta} \frac{\bar{q} \, Sref}{m \, VKTAS \left(\frac{6076}{3600}\right)} \tag{10}$$

and

$$N_r = Cn_r \frac{\bar{q} \, Sref \, b^2}{2 \, Izz \, VKTAS \left(\frac{6076}{3600}\right)} \tag{11}$$

Approved for Public Release – Case Number: 2022−0708

Note that $dCn/d\beta$, $dCl/d\beta$ and $dCY/d\beta$ are given in terms of per-degree while the dynamic derivative Cn_r representing the variation in airplane yawing moment coefficient with dimensionless change in yaw rate is given in radian/sec; they along with all of the mass moments of inertia are in body fixed axis.

Once again, we note the presence of the true airspeed in the denominator of both terms controlling the damping ratio. This is important for hypersonic flight because the damping ratio (holding the Dutch-Roll frequency constant) declines inversely proportional to $VKTAS$ given constant Cn_r and $dCY/d\beta$. In reality, since both Cn_r and $dCY/d\beta$ tend to decline with increasing Mach number, the loss of damping is more severe yet. Absent any sort of synthetic stability system, as airspeed increases from 200-KTAS to 4,000-KTAS (i.e., $M = 0.3 \rightarrow \sim6$), the damping will decline by a factor of at least 20. Thus, we see a need for closed-loop feedback augmentation to achieve satisfactory Dutch-Roll damping at very high airspeeds. Additional screening metrics need to be established to better infer the nature of aerodynamic control power (forces, moments and rates) associated with synthetic yaw damping.

D. Other Lateral-Directional Dynamics

The Roll-Mode is a first-order convergence/divergence seen as a tendency to damp roll rate when the commander executes a bank maneuver. The Roll-Mode is typically defined with the roll time constant, τ_R; this represents the time to achieve 63% of the peak roll rate based upon steady aileron input. τ_R is independent of the magnitude of the roll control input. If $\tau_R < 0$, the aircraft is unstable and behaves unpredictably to roll commands. If $\tau_R < 0.1$-sec, the airplane is extremely (possibly excessively) responsive to roll inputs. Conversely, if τ_R is too long, the airplane will respond so sluggishly to commanded roll inputs to degrade maneuvering performance. [21][22][23] The *LEVEL 1* boundary for flight is $\tau_R < 1.4$-sec; for *LEVEL 2*, $\tau_R < 3.0$-sec; for *LEVEL 3*, τ_R shall not exceed 10-sec. [19][29]

We may estimate τ_R by:

$$\tau_R \approx -\frac{1}{L_p} \tag{12}$$

where

$$L_p = Cl_p \frac{\bar{q}\, Sref\, b^2}{2\, Ixx\, VKTAS \left(\frac{6076}{3600}\right)} \tag{13}$$

Note that the dynamic derivative Cl_p represents the variation in airplane rolling moment coefficient with dimensionless change in roll rate; it is given in radian/sec. All aerodynamic and mass moments of inertia are in body fixed axis.

For slender, hypersonic vehicles, the mass moment of inertia Ixx tends to be relatively small as mass is concentrated near the vehicle centerline and the flight speed ($VKTAS$) is very large. The roll time constant will depend greatly then upon the flight dynamic pressure; at low dynamic pressures τ_R may prove to be objectionably long whereas at very high dynamic pressures τ_R may prove to be objectionably short.

The Spiral-Mode is another first-order convergence/divergence that manifests itself as a tendency to roll into an ever tightening spiraling turn (unstable) or roll out of a turn back to wings level flight (stable). [21][22][23] The unstable mode is a potentially dangerous divergence; the aircraft, when disturbed in yaw, displays a bank angle increase which locks the aircraft into an ever-tightening spiral. We may estimate τ_S by:

$$\tau_s \approx -\frac{1}{s} \tag{14}$$

where

$$s \approx \frac{L_\beta N_r - N_\beta L_r}{L_\beta + N_\beta \left(\frac{Ixz}{Ixx}\right)} \tag{15}$$

$$L_\beta = 57.3 \frac{dCl}{d\beta} \frac{q\, Sref\, b}{Ixx} \tag{16}$$

$$L_r = Cl_r \frac{\bar{q}\, Sref\, b^2}{2\, Ixx\, VKTAS \left(\frac{6076}{3600}\right)} \tag{17}$$

$$N_\beta = 57.3 \frac{dCn}{d\beta} \frac{\bar{q} \, Sref \, b}{Izz} \qquad (18)$$

$$N_r = Cn_r \frac{\bar{q} \, Sref \, b^2}{2 \, Izz \, VKTAS \left(\frac{6076}{3600}\right)} \qquad (19)$$

Note that $dCn/d\beta$ and $dCL/d\beta$ are given in terms of per-degree while the dynamic derivative Cn_r and Cl_r representing the variation in airplane yawing and rolling moment coefficient with dimensionless change in yaw rate are given in-radian/sec; they along with all of the mass moments of inertia are in body fixed axis.

When $s < 0$, the Spiral-Mode is stable; this is good. If $s > 0$, the Spiral-Mode is unstable. However, an aircraft can still have a satisfactory Spiral-Mode as long as this mode is not too unstable; $\tau_S < 4$-sec if $s > -0.25$. [19][29] While high speed *(VKTAS > 1000)* high altitude *(q < 35-lbf/ft²)* flight should lead to small s regardless of the aerodynamic derivatives we must be vigilant against spiral divergence issues at high dynamic pressures.

E. Bandwidth Concerns

Recall that the goal of the aircraft control system is to enable the commander to direct the aircraft to be able to fly where he so desires. That implies that any given aircraft should be able to successfully execute a set of "Standard Evaluation Maneuvers;" the Air Force has defined such sets for combat aircraft and identified key metrics which have been included in standards such as MIL-STD-8785C, MIL-STD-1797A and MIL-STD-1797B. [19][28][29] These maneuvers include: 1) significant (i.e., 50-KTAS) accelerations and decelerations to capture a new airspeed, 2) rolling maneuvers from rest through a specified bank angles, 3) ability to capture and stabilize steady heading sideslips.

MIL-STD-8785C and MIL-STD-1797B categorize aircraft based on their size and intended purposes: there are three categories of nonterminal flight of which we focus primarily on *CATEGORY A. CATEGORY A* flight implies active maneuvering whereas *CATEGORY B* is defined as "Climb" "Cruise" and "Loiter" (less demanding piloting conditions) or *CATEGORY C* which is defined for takeoff and landing (and is even more demanding to the pilot). [19][29]

MIL-STD-8785C and MIL-STD-1797B define three levels of "handling qualities" representing pilot workload as defined by the Short-Period frequency and pitch responsiveness of the airframe: *LEVEL 1* where the qualities are clearly adequate, *LEVEL 2* where flying qualities are adequate but requires a higher workload, and *LEVEL 3* where the aircraft is still safe but requires excessive workload. [19][29]

Mitchell, et al proposed revisions for a forthcoming MIL STD-1797C to suit diverse high-speed as well as non-aerobatic transport category aircraft including a "generic hypersonic aerodynamic model," the SR-71, the TU-144L and the F-16XL. In order to execute command maneuvers without objectionable phase lag, maneuvering bandwidth specifications will indirectly set a floor to the lower bound of acceptable rigid-body mode frequencies, time-constants and damping ratios. Mitchell notes that the "results of these studies … are not sufficiently mature to directly affect the current requirements in MIL STD-1797B." [30] While "there were also efforts to find alternative definitions, axes, or measurements for the existing criteria" there is a lack of "strong evidence that any of the existing criteria should be modified or new criteria adopted." [30]

An important parameter to track is airframe pitch responsiveness: [18][19]

$$\frac{n}{\alpha} \approx \frac{57.3 \frac{dCL}{d\alpha} q \, Sref}{W} \qquad (20)$$

Referring to TABLE 2, if pitch responsiveness is too low, excessive angle-of-attack will be needed to attain 1-gee flight. For example, $n/\alpha \sim 5$ implies flight where α is 11° above zero lift. A combat maneuverable airframe demands even higher values for n/α; $n/\alpha \sim 10$ implies 1-gee flight where α is 5.7° above zero lift and the 3-gee maneuver point is α is ~17° above zero lift. Thus, most maneuvering aircraft need to be designed to operate where $n/\alpha >> 10$.

MIL-STD-8785C and MIL-STD-1797 outline Stick-Fixed Short-Period frequencies for satisfactory flight; see Fig. 15. [19][28] The upper bound of the rigid-body Short-Period mode is one where the frequency is below that of primary structural resonance; typically, this will be a single digit frequency (i.e., 3-Hz) as predicted by structural finite-element-analysis. It is possible for this condition to develop when a very stable aircraft flies at extremely high dynamic pressure ($KEAS >> 1000$).

MIL-STD-8785C and MIL-STD-1797 (refer once again to Fig. 15) stipulates *LEVEL 1* qualities if the Control Anticipation Parameter (CAP), i.e., $\omega^2_{sp}/(n/\alpha)$, falls between $0.28 < \omega^2_{sp}/(n/\alpha) < 3.6$; with a floor of $\omega_{sp} = 1$-radian/sec (0.16-Hz or a 6.3-sec Short-Period mode). *LEVEL 2* qualities if $0.16 < \omega^2_{sp}/(n/\alpha) < 3.6$; with a floor of $\omega_{sp} = 0.6$-radian/sec (0.095-Hz or a 10.5-sec Short-Period mode). *LEVEL 3* qualities exist so long as $\omega^2_{sp}/(n/\alpha) > 0.16$. If $\omega^2_{sp}/(n/\alpha) < 0.16$ the aircraft is unacceptably unresponsive. [19][28]

Hypersonic Boost-Glide (X-15) and Reentry Vehicles (Shuttle) fly extremely high altitudes. Despite the high Mach number, this portion of hypersonic flight may occur at low dynamic pressure. Thus, we must consider the lower bounds of longitudinal responsiveness. As the aircraft leaves the atmosphere, q and n/α both trend towards zero.

For low-speed or quasi-ballistic flight, where the aircraft may operate $n/\alpha < 10$, we see that the minimum permissible *LEVEL 3* Short-Period frequency is ~0.4-radian/sec (a 15-sec period). When the Rigid-Body frequencies drop below that, the aircraft becomes hopelessly unresponsive to a pilot using a conventional control strategy. Under such circumstances, the GN&C system will need to abandon an aerodynamic control approach and revert to RCS.

TABLE 2 Physical interpretation of n/α

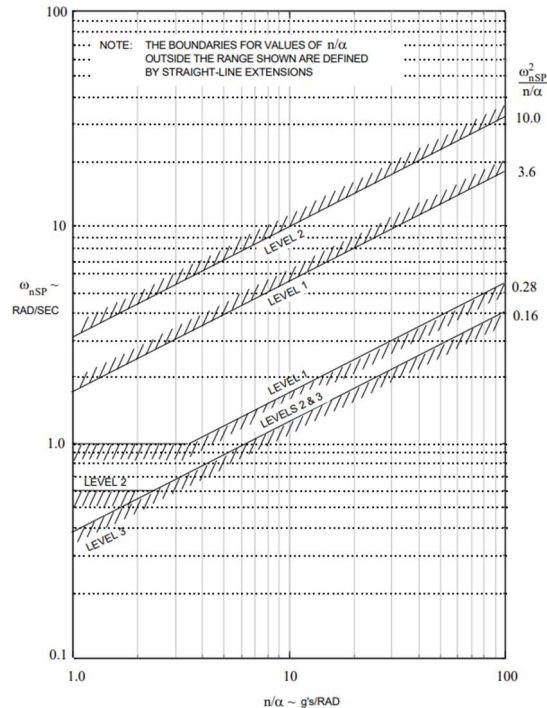| n/α (g/radian)	1-gee alpha (deg)	2-gee alpha (deg)	3-gee alpha (deg)
1	57	115	172
2	29	57	86
3	19	38	57
4	14	29	43
5	11	23	34
10	5.7	11	17
20	2.9	5.7	8.6
30	1.9	3.8	5.7
40	1.4	2.9	4.3
50	1.1	2.3	3.4
100	0.6	1.1	1.7

Fig. 15 MIL-STD-8785C *Short-period Frequency-vs-Pitch Responsiveness* (Control Anticipation Parameter) Chart for *CATEGORY A* Flight Phases [19]

We note that some closed-loop feedback control systems will display conventional, damped oscillatory behaviors amenable to MIL-STD-1797B style screening, while others do not. The forthcoming discussion of Space Shuttle Orbiter considers a vehicle with a complex feedback system that completely suppresses the classical Short-Period mode.

The longitudinal bandwidth needed for a "straight-and-level" propulsion testbed aircraft (like a X-43A or X-51A) is much less demanding than that needed to fly a general purpose aircraft over a typical mission. Mitchell concurs with

existing guidelines regarding short-period frequency and pitch responsiveness; refer to Fig. 15. [30] He also documents a degradation in pilot performance when the aircraft phase lag exceeds ~45°. Because a classical moderately damped system displays ~45° phase lag at ~75% of its natural frequency and since high-speed vehicles are unlikely to feature direct lift control (their longitudinal gee capability will be linearly proportional to the angle-of-attack), we may derive some minimum longitudinal bandwidth criteria as a function of inherent pitch responsiveness; see TABLE 3.

For *LEVEL 1* flying qualities, both MIL-STD-8785C and MIL-STD-1797A specify the short-period damping ratio $\zeta_{SP} > 0.35$ and under no circumstances should fall below $\zeta_{SP} < 0.15$. [19][29]

The requirement to examine the product of frequency and damping was first noted by Koven & Wasico, [20] who observed that the pilot preference for short-period damping-ratio correlated to the inherent frequency. They realized that the important metric was driven by energy dissipation rate rather than the number of oscillations after a disturbance; the faster the frequency, the weaker the damping could be before pilots would deem the aircraft unsafe to fly; see Fig. 16. Koven & Waisco [20] also noted the need for adequate pitch damping to "minimize 'hunting' and overshoots which occur when the pilot … changes pitch attitude." We note that MIL-STD-8785C does not specify a minimum energy dissipation rate ($\omega \cdot \zeta$) criteria for the longitudinal Short-Period but does specify one for the Dutch-Roll. [19]

Mitchell notes that "lateral-directional flying qualities are usually defined in terms of the basic lower-order modal characteristics of the free response, with some additional limits on time-domain measures of forced responses." [30]

TABLE 3 Minimum Longitudinal Bandwidth at 45° phase lag for *CATEGORY A* Flight Phases inspired by MIL-STD-8785C and MIL-STD-1797A.

n/α (g/radian)	Bandwidth Level I (radian/sec)	Bandwidth Level II (radian/sec)
1	0.75	0.45
2	0.75	0.45
3	0.75	0.52
4	0.79	0.60
5	0.89	0.67
10	1.25	0.95
20	1.77	1.34
30	2.17	1.64
40	2.51	1.90
50	2.81	2.12
100	3.97	3.00
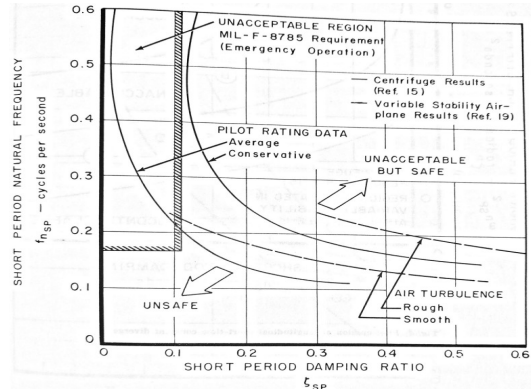
Fig. 16 Examining Energy Dissipation Rate of Dynamic Motion [20]

MIL-STD-8785C and MIL-STD-1797B suggest that high-speed combat aircraft have preferred (i.e., *LEVEL 1*) capability to roll from stable flight to accelerate in roll through a 90° change in bank angle in no less than 1.4-sec. It also suggests that non-maneuvering transport category aircraft have a preferred (i.e., *LEVEL 1*) roll capability to re-orient from wings level through a 30° bank angle in no less than 2.0-sec. To prevent excess phase-lag, Mitchell [30] suggests that even large transport aircraft have a roll-mode time constant, τ_R, < 0.8-sec; MIL-STD-8785C advises that τ_R > 0.1-sec to avoid an "over-control" situation from forming. [19][29]

In terms of the Dutch-Roll Mode, MIL-STD-8785C and MIL-STD-1797B suggest that the frequency, ω_{dr}, and damping ratio, ζ_{dr}, of the lateral-directional oscillations following a yaw disturbance input shall exceed the following minimums (for *LEVEL 1* controllability): ω_{dr} > 0.04-radian/sec (i.e., period should not exceed 15-sec), ζ_{dr} > 0.19, as well as a metric of net energy dissipation ($\zeta_{dr} \cdot \omega_{dr}$ > 0.35). Under no circumstances should residual limit-cycle oscillations exceed $\beta = \pm 0.17°$ (± 3 mils). [19][29]

F. Lateral-Directional Control-Coupling

Lateral-directional control-coupling occurs when commanded lateral rolling moments (*dCl/dail*) are accompanied by unintentional yawing moments (*dCn/dail*); this is an innate byproduct of aerodynamic control surfaces. Ideally the unintentional yawing moment is of the same sign as the rolling moment; what is known as proverse yaw-due-to-aileron. This allows a stable equilibrium to develop where the static directional stability (*dCn/dβ* > 0) at the developed sideslip angle (*β* < 0) opposes the yawing moment associated with the roll. In the favorable case, the innate static dihedral effect (*dCl/dβ* < 0) at the developed sideslip angle (*β* < 0) augments the commanded rolling moment. In the unfavorable case, the yawing moment is of opposite sign to the rolling moment; this is known as adverse yaw-due-to-aileron. This fosters an unstable equilibrium, where the static directional stability (*dCn/dβ* > 0) leads to a positive sideslip angle (*β* > 0) opposing the adverse yaw. If the innate static dihedral effect (*dCl/dβ* < 0) is strong enough at the developed sideslip angle (*β* > 0) it may overwhelm the commanded rolling moment and lead to an apparent "control reversal". A commanded right roll thus leads to a dynamic yawing motion which eventually results in a left roll. This dynamic mode is very difficult to arrest and is likely to lead to a loss of control of the vehicle.

The onset of control-coupling may be predicted by the Lateral Control Departure Parameter, *LCDP*:

$$LCDP = \frac{dCn}{d\beta} - \frac{dCl}{d\beta} \frac{\left(\frac{dCn}{dail}\right)}{\left(\frac{dCl}{dail}\right)} \tag{21}$$

If *LCDP* > 0, adverse yaw-due-to-roll is unlikely to lead to dynamic instability. If *LCDP* < 0, roll command inputs are likely to lead to a spin. Since slender, swept vehicles inherently have significant aerodynamic dihedral (*dCl/dβ* < 0), substantial static directional stability (*dCn/dβ* >> 0) is needed to resist any adverse yaw from the roll control aerodynamic surface to keep *LCDP* positive. [31][32] In the case study portion of the paper, we will see that *LCDP* is an effective discriminator to predict aircraft with debilitating controllability problems.

To reduce the amount of adverse yaw from the roll control surface, the *CAS* may implement complex "stick-to-surface" gain schedules; for example, an Aileron-Rudder-Interconnect (*ARI*). Weissman [31] discusses a revised departure parameter based upon a defined aileron-to-rudder-interconnect ratio, k_1:

$$LCDP = \frac{dCn}{d\beta} - \frac{dCl}{d\beta} \frac{\left(\frac{dCn}{dail}+k_1\frac{dCn}{drud}\right)}{\left(\frac{dCl}{dail}+k_1\frac{dCl}{drud}\right)} \tag{22}$$

Depending upon the configuration, a fractional movement of the yaw control surface may be able to neutralize the adverse yaw from the roll surface. Hypersonic vehicles, particularly if short coupled, may well feature substantial adverse roll from their rudder surfaces. On such a configuration, poor *LCDP* cannot be salvaged by *ARI* because the ensuing "force-fight" so degrades the attainable rolling moment to render other control metrics (such as time to roll) unacceptable.

Johnston et al [33] note that while *ARI* can produce more favorable *LCDP*, if the static aerodynamic cross-coupling is strong enough, the pilot can still drive the vehicle into a divergence which may exceed the sideslip limiters capability to respond. A related issue brought up in AGARD 336 [20] relates to the implied equilibrium sideslip angle (*β*) that develops in response to application of full roll control power). Koven & Wasico's discussion turns on the ratio, $\frac{\beta_{max}}{\dot{p}_{max}}$. We suggest, given the finite linearity of weathercock stability, that the appropriate screening parameter be written as:

$$\beta_{max} = \left| \frac{\frac{dCn}{dail}\delta ail_{ma}}{\frac{dCn}{d\beta}} \right| \tag{23}$$

For most aircraft, β_{max} should be limited so that the sideslip angle does not stall the vertical stabilizer; β_{max} < 10°. For high-speed air-breathing vehicles with inlets very sensitive to unstart, β_{max} should be limited to a much smaller value, perhaps less than ±1°.

A related cross-coupling metric is the $\frac{\phi}{\beta}$ ratio first considered by Carter in 1957. [31][34]. This represents the physical motion of the aircraft in response to a sideslip as the dihedral effect (*dCl/dβ*) and weathercock stability (*dCn/dβ*) are

viewed through the prism of mass moments of inertia. If $\frac{\phi}{\beta} \gg 1$, the response to a sideslip will present as a rolling motion; if $\frac{\phi}{\beta} \ll 1$, the response to a sideslip will present as a restoring yawing motion.

$$\frac{\phi}{\beta} = \left| \frac{\frac{dCl}{d\beta} \, Izz}{\frac{dCn}{d\beta} \, Ixx} \right| \qquad (24)$$

The authors are aware of the Kalviste Departure criteria [35] ; we note that his metrics are most applicable to flight at high sideslip angles. At modest sideslip angles, as expected on a Hypersonic platform, the traditional Bihrle-Weissman approach should be sufficient to identify unfavorable designs.

Bihrle-Weissman criteria have evolved over the years. This approach categorizes lateral-directional departure resistance in terms of both Dutch-Roll stability ($C_{n\beta dynamic}$) and *LCDP*. Weissman [31] found departure free characteristics for his studied aircraft (the F-4, F-111, A-7 and F-5) so long as *LCDP* was positive; see Fig. 17a (overleaf). MIL-STD-1797A [28] suggests a need for inherent Dutch-Roll stability ($C_{n\beta dynamic} > 0$); see Fig. 17b. We generally follow Mason [36] but include Skow's criteria from AGARD CP-235 [27] to set a less permissive lower boundary to $C_{n\beta dynamic}$; Skow suggests $C_{n\beta dynamic} > +0.004$ to guard against departure. We agree; we will use Fig. 17c as the reference for Weissman charts found elsewhere in this paper.
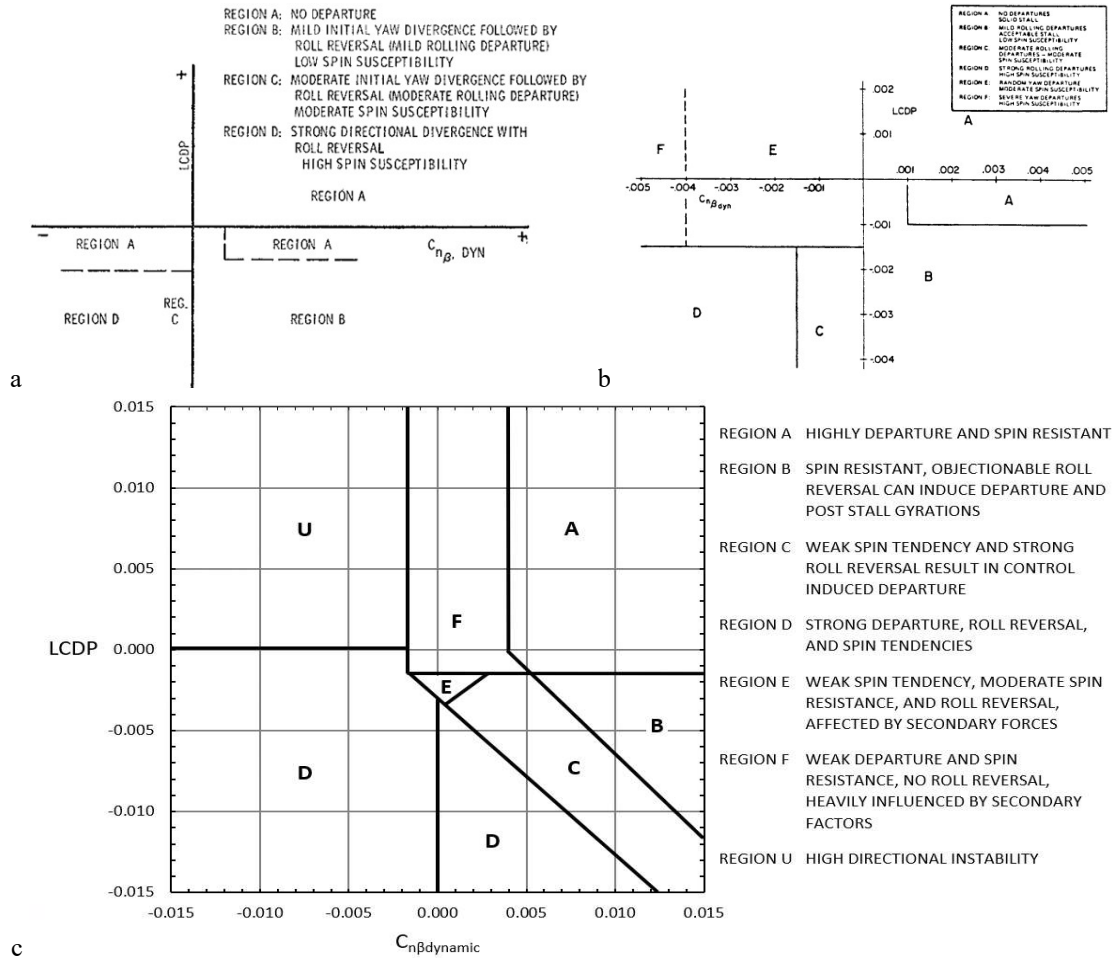
Fig. 17 – Evolution of Bhirle-Weissman Stability Criteria. a) Weissman from 1974 [31], b) MIL STD 1797A [28] c) Revised Version after WH Mason [36] and Skow [27].

G. Inertia Coupling and Frequency Coupling

When an airplane rolls about an axis which is not aligned with its longitudinal axis, inertia forces are introduced which tend to swing the fuselage in sideslip. Classical theory decouples the longitudinal (i.e., Short-Period and Phugoid) from the lateral-directional (i.e., Dutch-Roll, Roll and Spiral) modes. Reality proves to be more complex; energy can exchange between the longitudinal and lateral-directional Rigid-Body modes as well as between any Rigid-Body mode and an elastic structural mode.

Phillips in NACA TN-1627 from 1948 [37] noted that high-speed aircraft which "include short wing spans, fuselages of high density and flight at high altitude" tend to have rolling mass moments of inertia (Ixx) much smaller than their pitching (Iyy) or yawing (Izz) moments of inertia. In light of the full equations of motion, pitch acceleration ($\dot{q}$) includes components proportional to roll-rate (r) and yaw-rate (p). Similarly yaw acceleration ($\dot{r}$) includes components proportional to the pitch-rate (q) and yaw-rate (p). These forces are ordinarily neglected when the usual theory of lateral stability of aircraft is used to calculate the motion of an airplane in a roll. This assumption is probably justified for the case of most conventional airplanes because inertia forces involved are small compared with aerodynamic forces on the airplane; however, inertial forces manifest themselves as flight speed increases.

At minimum, it is always good practice to compute the ratio (Izz/Ixx). If this parameter is much greater than one, mass moments of inertia in yaw overwhelm those in roll; the vehicle is deemed "body heavy." If this parameter is much less than one, mass moments of inertia in roll dominate; the vehicle is deemed "wing heavy."

It is also useful to track the ratio, $\left|\frac{Ixx-Iyy}{Izz}\right|$, to gain insight as to how easy it is for oscillatory energy in the Short-Period to cross over into the Dutch-Roll. [37] When this term is near zero, there is no energy transfer between modes. The larger the magnitude of this term, the more pitch motions will excite yaw motions and vice-versa. Phillips [37] notes that a vehicle with $Ixx{\sim}0.4Iyy$ where $Iyy{\sim}Izz$ is highly prone to inertia couple; this corresponds to $\left|\frac{Ixx-Iyy}{Izz}\right| {\sim}0.6$.

Traditional design of control systems involves the inspection of Bode plots; which diagram the amplitude and phase response of oscillatory systems as a function of frequency. As Christopher Cotting at the USAF Test Pilot quips: "Linear Time Invariant systems are like toddlers playing with Legos – you want to keep them all separated otherwise bad things happen."[38] Since energy can exchange between the longitudinal and lateral-directional rigid-body modes as well as structural frequencies and control inputs, we must pay attention to congenital frequency coupling issues endemic to a configuration. Consider that an airplane rolling about an axis that is not aligned with its principal mass-moment-axis develops a resonant divergence in pitch or yaw when the roll rate is equal to the lower of the pitch or yaw natural frequencies. [7]

The designer must consider that Open-Loop and Closed-Loop control systems may demonstrate frequency coupling. These issues may manifest themselves when:

- The Short-Period lies too close to the Dutch-Roll mode; inertia coupling prone configurations may exhibit considerable energy exchange between modes [7]
- Pitch commands have spectral content near the Short-Period mode; pitch inputs may excite the Short-Period [7]
- Pitch commands have spectral content near the Dutch-Roll mode; inertia coupling prone configurations may excite Dutch-Roll from pitch command inputs [7]
- Roll commands have spectral content near the Short-Period mode; inertia coupling prone configurations may excide Short-Period from roll command inputs [7]

Fig. 18 Bode Plot for a lightly damped (ζ=0.19) linear system

- Roll commands have spectral content near the Dutch-Roll mode; this can lead to a "ratcheting" rather than smooth response to roll command [7]
- The Spiral-Mode lies too close to the Roll-Mode; this excites the Lateral-Phugoid mode [29][39]
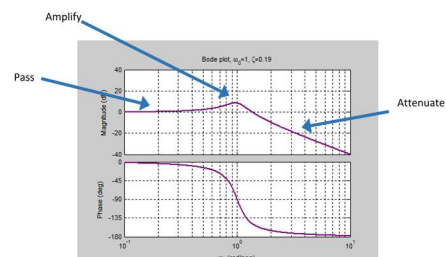
A quick look at a generic Bode pilot demonstrates the issue. The characteristic frequencies for Short-Period and Dutch-Roll represent turnover points for low-pass filters. Below its characteristic frequency the system passes inputs with unity or slight gain and modest phase lag. For example, the system in Fig. 18 has response lagging the forcing function by 45° at ~75% of the characteristic frequency. Thus, if a hypersonic aircraft featured a Short-Period frequency of ~2-radian/sec (i.e., ~3.1-sec period) command could give it control inputs with a ~1.5-radian/sec peak spectral content (i.e., nothing faster than a ~4-sec period) before encountering objectionable phase lag. There is some positive amplification right around the characteristic frequency. Above the characteristic frequency, the system response declines at 6-dB per octave (i.e., at double the characteristic frequency the response to the stimulus has been attenuated by a factor of 2). The system in Fig. 18 ($\zeta = 0.19$) features noticeable gain over a fairly broad range of frequencies (±30%) centered on the characteristic frequency. Given 1) that the equations of motion inherently cross couple the Short-Period mode to the Dutch-Roll Mode and 2) that hypersonic aircraft are inherently poorly damped, it is easy to how a longitudinal oscillation (ω_{SP}) can provoke a lateral-directional oscillation (ω_{DR}) that could drive the aircraft beyond its allowable sideslip limits. Similarly, control systems may drive Lateral-Phugoid oscillations when τ_S and τ_R align closely; this develops when aircraft have high effective dihedral ($dCl/d\beta << 0$) and low roll damping ($Clp \sim 0$). MIL-STD-1797 holds that Lateral-Phugoid behavior is impermissible in Category A flight. [28]

Equations 1 through 24 represent metrics that can be computed directly from aerodynamic data available during the early design. In subsequent sections we will show how they predicted stability and control successes and failures across a variety of high-speed aircraft.

V. Case Studies

In this section, we review wind tunnel and flight test data for diverse vehicles such as the rocket propelled Bell X-2 and North American X-15, the Martin X-24A and Northrop HL-10 lifting bodies, the Lockheed YF-12 (SR-71) and North American XB-70 jet propelled aircraft as well as the Rockwell Space Shuttle Orbiter. Much more limited data exists in open forums concerning more recent high-speed vehicles including the DARPA/Lockheed HTV-2 and DARPA/AFRL/Boeing X-51A programs; see FIGS. 2,3 and 19 through 24.

We note that the X-2, YF-12/SR-71 and XB-70 were high supersonic aircraft. While not test-flown at hypersonic speeds, the X-24A and HL-10 were configured as viable atmospheric reentry vehicles and flew a successful envelope expansion flight test program. Alternatively, we understand that recent hypersonic vehicles such as the X-43A, HTV-2 and X-51A are "limited envelope" technology demonstrators. Finally, the X-15 and Space Shuttle Orbiter were successful general purpose hypersonic airframes with 199 and 135 missions flown respectively.

All these airframes are configured as bank-to-turn "airplane-style" vehicles, and as such are not designed to operate at significant sideslip angles at speed.

Fig. 19 Bell X-2

Fig. 20 Martin X-24A

Fig. 21 Martin X24-B

Fig. 22 Northrop HL-10

Fig. 23 Lockheed YF-12

Fig. 24 North American XB-70

Fig. 25 Lockheed HTV-2

A. Mass Properties

Reported mass properties from aircraft with complex flight test programs vary somewhat from flight to flight. In TABLE 4, we summarize nominal values from a range of reported values found in flight test. The reader should focus on the key ratios: Izz/Ixx and $\left|\frac{Ixx - Iyy}{Izz}\right|$.

All of these aircraft are "body heavy;" their mass-moments-of-inertia in pitch and yaw are much greater than roll. The X-24A lifting body is the least body heavy configuration considered; with $Izz/Ixx \sim 5.0$. The X-15 when fully fueled in the most body heavy configuration considered; with $Izz/Ixx \sim 24$. The other vehicles tend to fall between $5 < Izz/Ixx < 10$. In contrast, a large transport like a Lockheed C-5 has $Izz/Ixx \sim 2$. [16]

TABLE 4 Mass Moment of Inertia for High Speed Vehicles

	Ixx (slug-ft^2)	Iyy (slug-ft^2)	Izz (slug-ft^2)	Izz/Ixx	$\left\|\frac{Ixx - Iyy}{Izz}\right\|$
Bell X-2 [40]	5,000	25,500	29,000	5.7	0.70
North American X-15 [41]	3,600→ 5,200	85,000→ 108,000	86,500→ 110,500	21→ 24	0.93→0.94
Martin X-24A [42]	1,450→ 1,900	8,300	9,000→ 9,400	5.0→ 6.2	0.68→0.76
Northrop HL-10 [16]	1,350	6,400	7,400	5.5	0.68
Lockheed YF-12/SR-71 [43]	~220,500	~955,000	~1,172,000	5.3	0.63
North American XB-70 [44]	~2,600,000	~22,000,000	~24,000,000	11.9	0.61
Rockwell Space Shuttle Orbiter [45]	1,200,000→ 1,225,000	8,905,000→ 9,435,000	9,305,000→ 9,845,000	7.7→ 8.1	0.82→0.83

All of these vehicles with documented mass properties have a strong innate propensity to inertia couple, as $\left|\frac{Ixx - Iyy}{Izz}\right|$ lies between 0.6 and 0.9. Whereas a large transport like a Lockheed C-5 has as $\left|\frac{Ixx - Iyy}{Izz}\right| \sim 0.07$. [16] Thus slender vehicles, unlike transport aircraft, will crosstalk any energy found in a lightly damped longitudinal mode into the lateral-directional. Similarly, inertia coupling prone configurations will crosstalk any energy found in a lightly damped Dutch-Roll Mode into the longitudinal.

Although details of the aerodynamics and mass properties of the X-43A, HTV-2 and X-51A remain closely held, cursory inspection reveals slender geometries similar to our other documented high speed vehicles. Thus, with they also appear to be strongly "body heavy" and otherwise prone to inertia coupling.

B. Longitudinal Trim

None of the aircraft studied reports significant mission failures or need for re-design resulting from a lack of longitudinal trim. By the time the flight outer-mould-line was finalized, engineers correctly sized the longitudinal control surfaces to provide reasonable pitch authority throughout the flight envelope. This does not mean that ground-test and computation precisely matched flight-test experience.

We note three discrepancies in our survey. First Wolowicz & Yancey [46] note pilots reported elevator saturation issues during approach, landing-flare and touchdown during the NASA XB-70 flight test program; see Fig. 26.
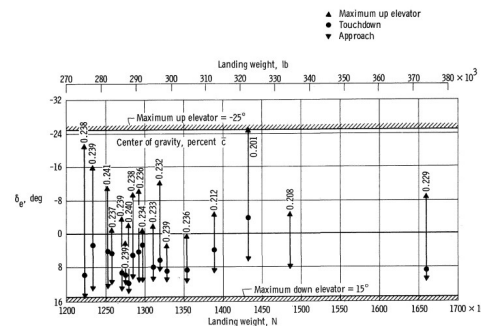
Fig. 26 XB-70 landing control power saturation [46]

Second, Layton [47] describes moderate pitch trim anomalies on the HL-10; see Fig. 27. Third, Kirsten, Richardson & Wilson [48] document how the body flap deflection needed to trim the Space Shuttle Orbiter differed substantially from pre-flight expectations; see Fig. 28.

Kirsten, et al noted that the Orbiter pre-flight big-picture aerodynamic performance assessment was satisfactory. [48] They found that "the hypersonic lift-to-drag ratio (L/D) data obtained from pushover-pullup maneuvers… showed excellent agreement with predictions." [48] At low speeds, the Orbiter over-performed with a "higher-than-predicted L/D out-of-ground effect … due primarily to the lower-than-predicted drag coefficient" arising from an "overprediction of the drag due to surface irregularities in the Thermal Protection System (TPS)." [48]

For the Orbiter, Kirsten, et al found "significant error in longitudinal trim in the hypersonic Mach regime" between pre-flight and flight test. [48] Theses anomalies were "apparent on all five Orbiter reentries. For example, during STS-1 the trim bodyflap was 16° rather than 7° at Mach numbers greater than 17." They found that "the major contributor to the trim error was an error in the basic pitch curve Cm_0." The Orbiter stability generally matched ground-test estimates; "the Orbiter was statically stable and the slopes indicated that the combined elevator effectiveness/pitch static stability was close to predictions." The need for additional longitudinal pitch control power was "attributable to an error in basic pitching moment (Cm_0)." They believe that the "primary cause of the error in the predicted hypersonic values of Cm_0 is felt to be real gas effects ... [which] were not fully simulated in wind tunnel tests."

B. Longitudinal Stability

Wind-tunnel and flight test data for the Bell X-2, North American X-15, the Martin X-24A, Northrop HL-10, Lockheed YF-12 (SR-71), North American XB-70 and Rockwell Space Shuttle Orbiter confirm designs with inherent longitudinal static stability; $dCm/d\alpha < 0$; see Figs. 29, 30 and 31. [16][49][50]

Fig. 27 HL-10 pitch trim anomalies [47]
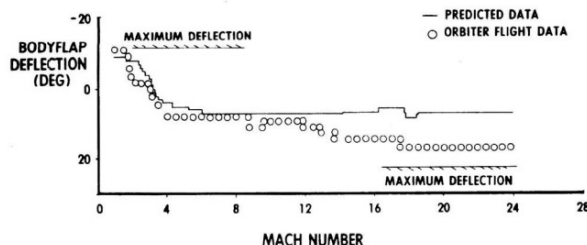
Fig. 28 Shuttle Orbiter pitch trim anomalies [48]
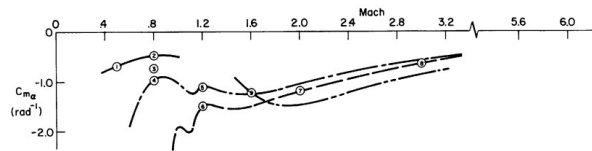
Fig. 29 X-15 Static Longitudinal Stability [16]
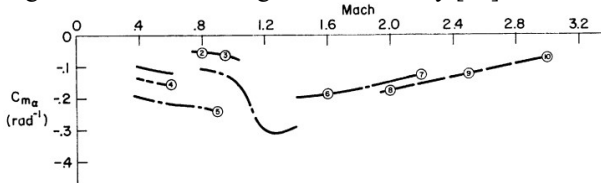
Fig. 30 XB-70 Static Longitudinal Stability [16]
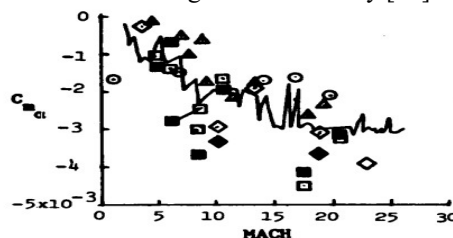
Fig. 31 Shuttle Orbiter Static Longitudinal Stability [50]

We next consider how well these high-speed aircraft satisfy the MIL-STD-8785C Short-Period Frequency vs. Pitch Responsiveness "Control Anticipation Parameter" criteria; refer back to Fig. 15.

19

Consider first the X-15. Note that it was flown at high speeds within the atmosphere and on exo-atmospheric "reentry" missions; see Fig. 32. The CAP chart (see Fig. 33) contains direct flight test data points from a variety of low altitude missions sourced from Ref. 49 as well as data prepared by Griffin & Takahashi. [12] While the basic low-altitude properties of the X-15 are firmly within the *LEVEL 1* region, on an exo-atmospheric mission as the vehicle leaves and initially re-enters the atmosphere the dynamic pressure drops so low as to render both pitch responsiveness and the Rigid-Body frequencies unacceptable despite maintaining the control anticipation parameter ($\omega^2/(n/\alpha)$) within *LEVEL 1* guidelines. For this flight, it appears that the pitch responsiveness becomes unacceptable ($n/\alpha < \sim 3$) before the rigid-body frequencies drop below acceptable minimums. In other words, the X-15 has insufficient wing area to "glide" at $n_z = 1$ before the longitudinal handling qualities become hopelessly unresponsive.

Next consider the X-2; see Fig. 34. Its stick-fixed inherent longitudinal flying qualities are firmly in *LEVEL 1*. [51]

The X-24A, while largely sharing its outer-mould-line with the atmospheric reentry X-23, was flown 28 times at speeds up to $M = 1.6$ and at altitudes up to 71,400-ft. Longitudinal data flown with the pitch *SAS* intentionally disabled (or "adjusted" based on *SAS* enabled data) found inherent frequencies and pitch responsiveness well within *LEVEL 1* guidelines; see Fig. 35.

The HL-10 outer-mould-line, while being designed for atmospheric reentry, was flown 37 times at subsonic, transonic and supersonic speeds (M<1.86). Flight test did explore low-dynamic-pressure limits with one supersonic flight to 90,300-ft. Longitudinal data, flown with the pitch *SAS* intentionally disabled, revealed inherent frequencies and pitch responsiveness well within *LEVEL 1* guidelines; see Fig. 36, overleaf. [16] However, the flight test program was not without issues. The first flight was plagued by excessive longitudinal stick gains and presence of *SAS* induced 2.75-Hz longitudinal oscillations as well as a "lack of longitudinal and lateral-directional control at some portions of the flight." [53] After extending and re-cambering the leading edges of the outboard fins, revising *SAS* gains and logic, the HL-10 gained satisfactory longitudinal handling qualities. [53]

Over many years, NASA conducted "extended flight tests" of the YF-12 as well as SR-71 "Blackbird" aircraft. For the YF-12, pilots experimented with supersonic flight with "pitch *SAS* off and with roll and yaw *SAS* off, but never with pitch and yaw *SAS* off at the same time." [54] They note that with the "pitch *SAS* off, the Short-Period is not as well damped," as it was with the *SAS* enabled. [54] However, they found that the "decrease in damping is not immediately apparent to the pilot during cruise conditions." [54] Once again, longitudinal data, flown with the pitch *SAS* intentionally disabled, documented inherent frequencies and pitch responsiveness well within *LEVEL 1* guidelines; see Fig. 37, overleaf. With the *SAS* enabled, the Blackbird "will hold speed and altitude well if not disturbed … [but] small pitch attitude changes not immediately apparent to the pilot occur, and by the time the pilot notices it, a moderate altitude change is underway." [54]
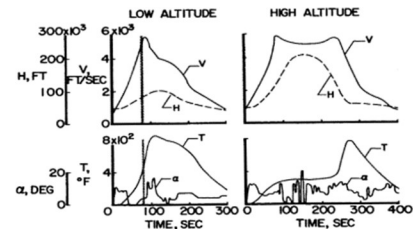

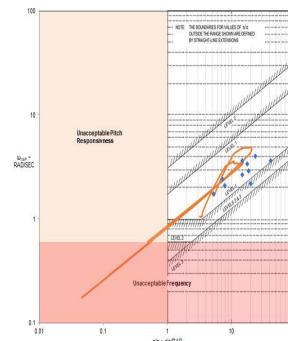Fig. 32 North American X-15 Example Flight Profiles [52]

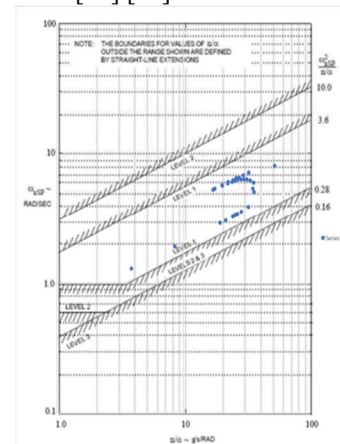Fig. 33 North American X-15 8785C chart [12] [16]

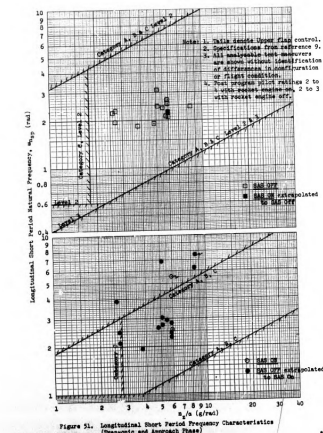Fig. 34 Bell X-2 reverse engineered 8785C chart [51]
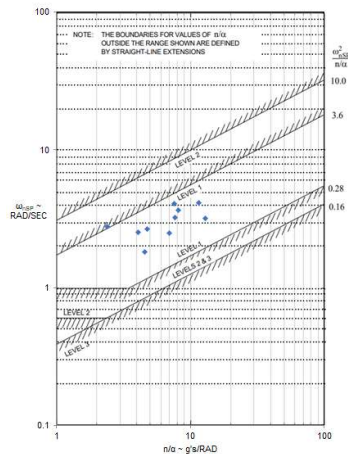

Fig. 35 Martin X-24A 8785C chart

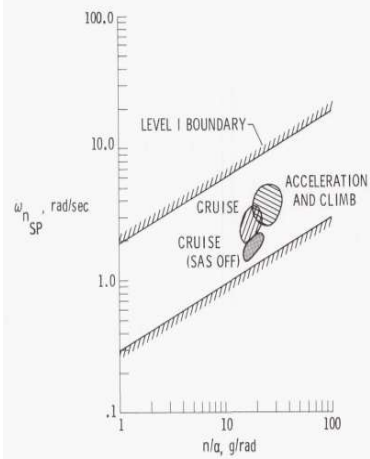Fig. 36 Northrop HL-10 8785C chart – *SAS* off [16]

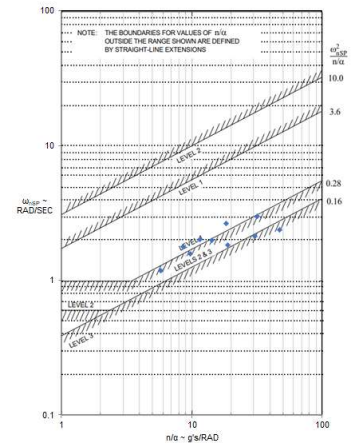Fig. 37 Lockheed YF-12 / SR-71 8785C chart [54]

Fig. 38 North American XB-70 8785C chart – *SAS* off [16]

Stitch, Sachs & Cox [25] explain these motions as a result of an interaction of the Phugoid with a previously neglected dynamic mode called the Height-Mode. The Height-Mode drives an instability in altitude and airspeed driven by the altitude dependence of propulsion system performance. [25] If the Height-Mode time constant lies close to the Phugoid mode it destabilizes even gentle maneuvers such as a simple heading change at constant altitude and KEAS. [25] Suppressing this mode requires a complex control algorithm including pitch and throttle.

NASA ran a crash foreshortened flight test program of two XB-70 aircraft. [46] The XB-70-1 had an irreversible, powered flight control system actuating a variable incidence canard with trailing edge flap, 14° elevons on the trailing edge of the main wing, twin all moving vertical tails with 45° hinge lines and variable dihedral "droopable" wingtips. NASA found the XB-70's "inherent longitudinal stability and control characteristics [to be] generally satisfactory." [54] The major deficiency, noted previously, was available elevator control power during landing. Otherwise, NASA found the unaugmented short-period dynamics to be satisfactory, and "the correlation between flight data and predicted results to be generally good." [46] Fig. 38 shows the frequencies and pitch-responsiveness to be a bit lower than ideal for *LEVEL 1*, but still within *LEVEL 2* guidelines. Pilots reported that "response in pitch was quite slow." [55]

The AGARD CP-106 discussion forum cites D.T. Berry of NASA/Armstrong stating that the correlations between ω_{SP}^2 and n/α (the 8785C Control Anticipation Criteria) and pilot feedback for both the YF-12 and XB-70 flight research programs was good. [56]

The Space Shuttle Orbiter has a complex flight control system including reaction-control thrusters; during gliding flight, "the body flap is the predominant longitudinal trim device, while the wing-mounted elevons are used for longitudinal stability" and control. [50] "Aerodynamically, during the major portions of the flight from entry to touchdown, the vehicle is longitudinally … stable." [50] With such a complex algorithm, the Orbiter engineering team did not call out oscillatory frequencies or damping ratios.

As discussed previously, at high flight speeds, aerodynamic pitch damping declines precipitously. The effective damping ratio, ζ_{SP}, falls far below established norms in the absence of some form of stability augmentation system.

We believe that the X-2 lacked an electronic pitch *SAS*, but probably included a mechanical bob-weight / down-spring mechanism as such was common design practice during its era. Day wrote that "the damping of both the longitudinal and lateral modes was poor." [40]

We believe that the other survey airframes all featured some form of fly-by-wire control systems with pitch rate (q or $\dot{\theta}$) feedback controls.

The X-15-1 and X-15-2 (serial numbers 56-6670 and 56-6671) used a pilot-selectable "fixed-gain" three-axis *SAS* with rate gyro feedback having a range of ten preset gains in each axis available for pilot selection during flight. [57] Pilots were expected to "adjusting *SAS* gains during flight to maintain acceptable handling qualities." [57] The later X-15-3 was fitted with the MH-96 adaptive gain feedback controller for its aerodynamic surfaces; [58] For normal "stick-and-rudder" flight, this system synthesized pitch-rate damping with or without acceleration feedback. It could also command pitch-attitude and angle-of-attack-attitude holds. [58] The MH-96 also enabled automatic blending of the reaction controls and aerosurfaces during atmospheric exit and reentry. [57] When the autopilot aerodynamics gains reached 90% of their maximum sum, the system would enable the reaction control jets. It would discontinue reaction control augmentation when the aerodynamics gains fell below 75% of maximum. Failure of this system due to electrical arcing of another piece of instrumentation appears to be the proximate cause to the fatal crash of the X-15-3 on Flight 3-65. [57]

Layton [47] generalizes the lifting bodies longitudinal handling qualities with the remark "conventional handling-qualities criteria … apply reasonably well to these vehicles."

NASA flight tests document that the X-24A had satisfactory damping with the *SAS* off, $\zeta_{SP} \sim 0.4 \rightarrow 0.8$, at low speeds. At high speeds, $\zeta_{SP} \sim 0.1 \rightarrow 0.15$ with the *SAS* disengaged which was clearly inadequate. [42] With the *SAS* engaged, pilots reported that the "longitudinal handling characteristics of the X-24A … were generally well-behaved. Short-Period frequency and damping were adequate for all configurations flown." [42]

The HL-10 had a simple pitch rate feedback controller; Fig. 39. *SAS* disengaged, the HL-10 had very poor pitch damping; $\zeta_{SP} \sim 0.17$ at low speeds and altitudes declining to $\zeta_{SP} \sim 0.03$ at $M = 1.5$ and 72,000-ft. [16] With the revised *SAS* engaged, pilots deemed the HL-10 to have the "best flying of the lifting bodies." [53] Pilot comments on executing a pushover-pullup maneuver were ecstatic; "it was just so straightforward and pretty … extremely smooth and comfortable … pitch damping was fantastic." [42]

The YF-12 is "normally operated with a stability augmentation system (SAS) engaged to provide artificial stability in pitch and yaw, and damping in pitch, yaw, and roll." [54] With the *SAS* engaged, the aircraft exhibited poor speed stability that requires considerable pilot effort to set up a trim or cruise condition. [54] Once set, the aircraft "will hold speed and altitude well if not disturbed." [54] Fig. 40, reproduced from Ref. 52, shows the natural decline in damping ratio with Mach number; $\zeta_{SP} \sim 0.1$ at $M = 3$ cruise. This Fig. also shows how the pitch *SAS* provides enough synthetic Cm_q so that the YF-12 exceeds MIL-STD-8785C short-period damping requirements at all speeds and altitudes.

For the XB-70, NASA flight test found solid damping in the subsonic region ($\zeta_{SP} \sim 0.5$) and light damping of the order of $\zeta_{SP} \sim 0.10 \rightarrow 0.15$ in the high supersonic region; see Fig. 41. [46] NASA found that the pitch augmentation system further enhanced the short-period damping of the airplane in the subsonic Mach number region. [46] At high supersonic speeds, the poor unaugmented damping "gave the pilot a feeling of deadbeat response to longitudinal disturbances." [46] The report does not give a precise value for the augmented Short-Period damping, but time-histories of disturbances made at $M = 2.5$ indicate $\zeta_{SP} > 0.5$ at high speeds with the pitch *SAS* engaged. [46]
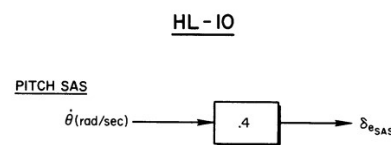

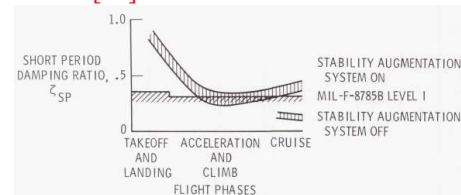Fig. 39 Pitch *SAS* Block Diagrams for the HL-10 [16]

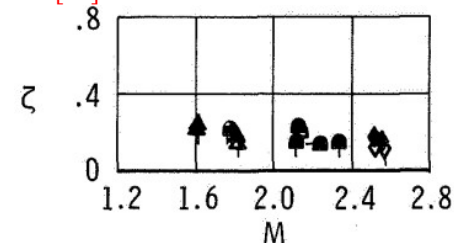Fig. 40 Short-Period Damping of the YF-12. [54]

Fig. 41 Short-Period Damping of the XB-70 in the supersonic configuration (wingtips drooped 65º) – SAS Off [46]
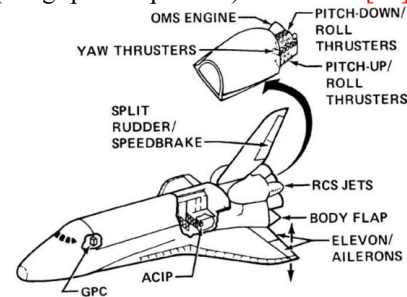

Fig. 42 Shuttle Orbiter Aerodynamic & Reaction Control System Configuration [11]

The Space Shuttle Orbiter Flight Control System (FCS) provides augmentation for both longitudinal and lateral directional axes throughout the entry profile. [59] Angle-of-attack and pitch-rate feedback provide stability augmentation and damping for the pitch axis. [59] The flight control gains are scheduled as a function of Mach number, angle-of-attack and dynamic pressure and are designed to provide "good flying qualities" throughout entry. [59] As with the X-15-3, the flight control system blends the use of aerodynamic and reaction control jets; see Fig. 42, prior page. [11] While early Orbiter documentation discusses a need to engineer the airframe to conform with MIL-STD-8785C *LEVEL 1* longitudinal pitch responsiveness and damping standards during terminal maneuvers, [60] little attention to these standards has been found in post-flight data reduction reports. [1]

None of the reports examined expressed any concern with the Phugoid mode frequency or damping.

Taken together, these experiences indicate that a vehicle which meets existing MIL-STD-8785C longitudinal short-period frequency and damping guidelines exhibits low-risk behavior in flight test. [19] Inherent with high-speed flight comes the need for synthetic pitch-damping. While no survey airframes exhibited satisfactory flying qualities at high speeds with pitch *SAS* disabled; all could successfully implement simple rate (q or $\dot{\theta}$) feedback controls. X-15 and Shuttle Orbiter demonstrated blending of reaction control and aerodynamic surface movement during flight at low dynamic pressure.

C. Inherent Lateral-Directional Stability and Control-Coupling Issues

Lateral-Directional stability and control issues prove much more challenging to the high-speed design community. Many programs discuss needs for significant redesign or envelope limitations resulting from lateral-directional aerodynamic deficiencies. Recall that aircraft remain "top side up" when they display stable oscillatory Dutch-Roll motions which does not absolutely require static directional stability ($dCn/d\beta > 0$). Due to the intrinsic loss of directional stability with increasing Mach number, and a desire to keep vertical tail volumes low, many high-speed designs were intentionally built to have only marginal directional stability.

In the following survey, we see from history that when marginal control was accepted; crashed airframes litter the desert. Here we present new Bihrle-Weissman and maximum sideslip analysis based on aerodynamic data from designs that predate development of these important screening criteria. Future designs need to learn from history and accept the intrinsic need for inherent static directional stability.

Let us begin with the X-2; recall Fig. 18. The flight test program terminated after a fatal crash on a Mach 3+ flight attempt. The proximate cause of the crash was control-coupling leading to a supersonic spin. Strong propulsion performance, inertial coupling and a lack of pilot familiarity with the airframe were contributory reasons. [40][51]

The X-2 has a stable Dutch-Roll mode ($C_{n\beta dynamic} > 0$), at low angles-of-attack, for $M < 3.2$. From Fig. 43, we see that the Bell X-2 with its swept wing exhibits noticeable effective dihedral ($dCl/d\beta < 0$) while maintaining some level of positive directional stability ($dCn/d\beta > 0$).

Fig. 43 Lateral & Directional Stability of the Bell X-2. [40]

The X-2, however, has insufficient vertical tail volume. From $M \sim 1.2 \rightarrow 1.8$, the static directional stability halves from $dCn/d\beta \sim 0.18$/radian to 0.09/radian; $0.003/°$ to $0.0015/°$. On a high-speed flight $C_{n\beta dynamic} > 0$, but barely exceeds $C_{n\beta dynamic} \sim +0.004$. Consider next the Bihrle-Weissman chart for the X-2; see Fig. 44. Due to adverse yaw from the ailerons and weak static directional stability, the vehicle is in the revised "F" region throughout its planned flight profile: "*F: weak departure resistance heavily influenced by secondary factors.*" [36] Careful examination of the yaw-to-roll ratio of the aileron reveals adverse yaw trends rising with both angle-of-
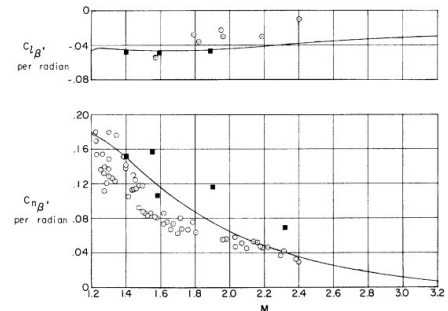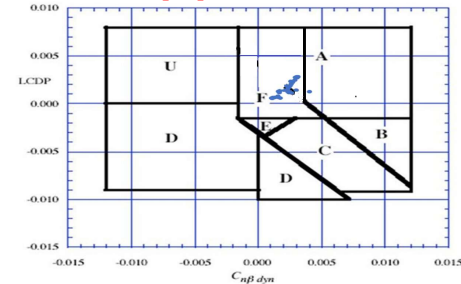

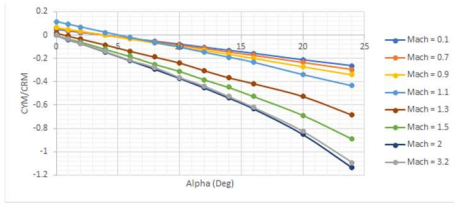Fig. 44 Weissman Plot of the X-2 [51]

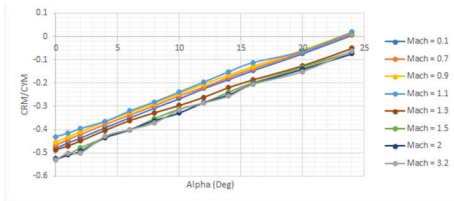Fig. 45 X-2 Aileron Yaw-to-Roll Ratio [51]
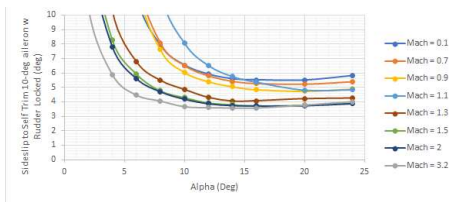

Fig. 46 X-2 Rudder Roll-to-Yaw Ratio [51]

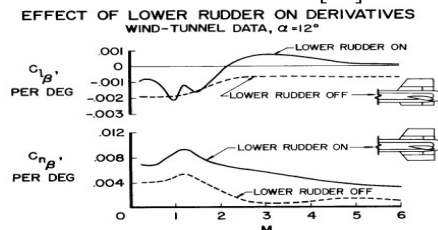Fig. 47 X-2 Sideslip to Self-Trim 10° Aileron with Rudder Locked [51]

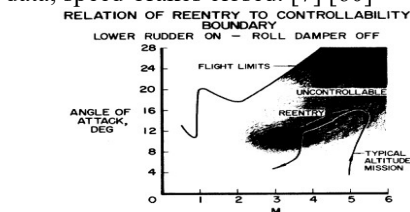Fig. 48 X-15 lateral-directional wind tunnel data; speed-brakes closed. [7] [60]

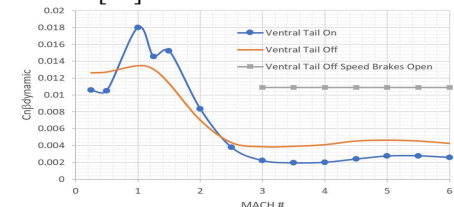Fig. 49 X-15 Lateral-Directional Controllability Boundaries with Large Ventral. [61]

Fig. 50 X-15 Configuration comparisons seeking to maximize $Cn\beta dynamic$ [60]

attack and Mach number; see Fig. 45. At $\alpha = 10°$ and $M \sim 3$, differential aileron produces approximately 40% as much yaw as roll. [51]

In light of the mass properties noted in TABLE 3, we can infer that the Dutch-Roll will express itself as wing rock at many flight conditions since $\frac{\phi}{\beta} \gg 1$ for all supersonic conditions.

Generally speaking, engineers would fit an aircraft that develops so much inherent adverse with ARI to reduce the problem to more manageable levels. Fig. 46 shows the challenge facing engineers in the era predating "fly-by-wire" control systems; the yaw-to-roll ratio of the rudder shows equally strong angle-of-attack trends. In order to cancel the adverse yaw of the ailerons, the flight control system would need to schedule rudder as a function of both Mach number and angle-of-attack. Since this level of flight control complexity was beyond the state-of-the-art in the late 1940's when Bell engineered the X-2, engineers decided to "lock" the rudder during high-speed flight and only enable its use for turn-coordination and sideslip trim during the terminal subsonic glide. [7]

This leads to the "fatal flaw" of the X-2 flight control system. With the rudder disabled, the adverse yaw from the ailerons causes any roll control inputs to drive the airframe to sideslip. Across a wide range of speeds and altitudes, 10° of aileron input implies a steady-state sideslip trim angle $\alpha > 10°$; see Fig. 47. It is no surprise that a pilot, when faced with a need to bank to turn at a flight speed above Mach 3, would accidentally induce a spin. [51]

The X-15 flight test program revealed additional issues concerning lateral-directional flight dynamics. As originally configured, the X-15 had a very large vertical tail volume with dorsal and ventral fins. This provided extremely strong static directional stability at the expense of dihedral effect; see Fig. 48. [7][61] As the flight test program continued and the X-15 was flown to greater speeds and over a wider range of angle-of-attack, pilots and engineers noted the weak Dutch-Roll stability; "poor handling qualities at the high angles of attack was due primarily to the large negative dihedral effect (positive $dCl/d\beta$) caused by the presence of the lower ventral fin." [61] For planned reentry missions, the combination of declining Dutch-Roll stability, the change in sign of the dihedral effect and weakening lateral-directional damping made the airframe uncontrollable without a functioning SAS; see Fig. 49. [62]

Beginning in late 1962, the X-15 was typically flown with the lower rudder removed. During atmospheric reentry, pilots operated the X-15 with "speed-brakes" open; it increased the wedge angle of the lower half of the ventral fin. In addition to providing much needed drag to prevent an "atmospheric skip," the speed-brake increased static directional stability considerably. With the lower rudder removed but speed brakes deployed; $dCn/d\beta \sim +0.008$. Fig. 50 compares the $C_{n\beta dynamic}$ trend with Mach number between large ventral, small ventral and small ventral with speed-brake deployed. We see how leaving off the lower rudder doubles $C_{n\beta dynamic}$ despite the reduction in static directional stability; even with speed-brakes

closed the X-15 now satisfies Skow's criteria ($C_{n\beta dynamic}$ > +0.004). Dutch-Roll stability improves even more at hypersonic speeds with the small ventral and deployed speed-brake.

Turning next to the Weissman chart (see Fig. 51) which demonstrates that the X-15 has strong departure resistance at all speeds and attitudes; all data is firm ly in the "A" region. The strong static directional stability (even with the lower rudder removed, so long as the speed-brakes are deployed above Mach 3) masks any adverse yaw from the "aileron" effect of differential horizontal tailplane. These changes increased the envelope limits of controllable flight substantially; consider Fig. 52, in contrast with Fig. 49.

With these configuration changes, the X-15 went to have a largely successful flight test program of 199 flights including many astronaut wings flights and speed records. The only fatal mishap of the X-15 program occurred on the 191st of 199 flights. [58] A cascading series of electrical anomalies resulted in an unrecognized failure of the *SAS* during rocket powered boost. [58] Pilot Michael Adams died after the aircraft departed flight in a lateral-directional spin. [58]

The X-24A and HL-10 lifting body configurations have many similar lateral-directional characteristics. They have relatively high dihedral effect ($dCl/d\beta$ << 0); they are also "wing heavy" (Izz/Ixx > 5). [63] Even though these configurations are festooned with many vertical and/or canted fins, they have relatively weak static directional stability; Figs. 53-54.

The operational challenge with these aircraft stems from a need to fly the aircraft at relatively high angles of attack. Turning next to Fig. 55, we see that much of the X-24A flight test program had the airframe operate at attitudes where the vehicle lacked any intrinsic static directional stability, i.e., above its $N_\beta = 0$ boundary but did not exceed the $C_{n\beta dynamic} = 0$ limit. As with the X-15, as the angle-of-attack increases, the dominant contributor to $C_{n\beta dynamic}$ arises from their effective dihedral, not from their static directional stability. On an ordinary, swept wing airplane this would not pose any problem but the HL-10, like other lifting bodies, has unusual aerodynamic dihedral characteristics.

If we examine the Mach 2.16 wind-tunnel run of the HL-10 with the revised "Mod II" vertical fins (return to Fig. 54) we see only weak aerodynamic dihedral. [64] This is due to the vertical disposition of directionally stabilizing elements. Dorsal vertical elements will produce effective dihedral ($dCl/d\beta$ < 0) while ventral vertical elements oppose this ($dCl/d\beta$ > 0). Thus, the HL-10 being a thick lifting body with multiple short vertical fins, demonstrates a peculiar dihedral effect trend: $dCl/d\beta$ ~ -0.001/deg relatively invariant to α, along with directional stability that declines as α increases.
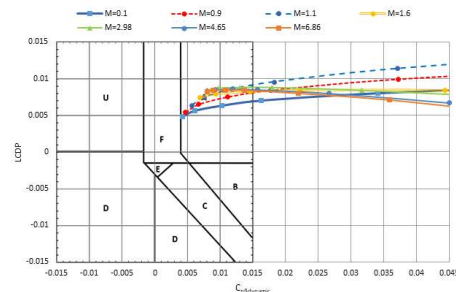

Fig. 51 X-15 Weissman Chart – small ventral. Total flight Envelope Data. Speed brakes above M>3. [12]
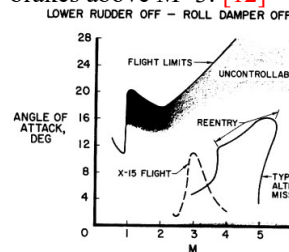

Fig. 52 X-15 Lateral-Directional Controllability Boundaries with Roll-Damper-Off [60]

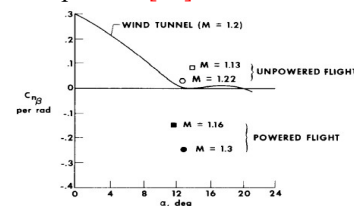
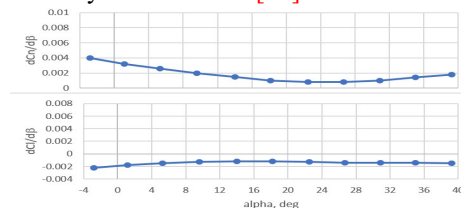Fig. 53 Low Supersonic Static Directional Stability of the X-24A [62]

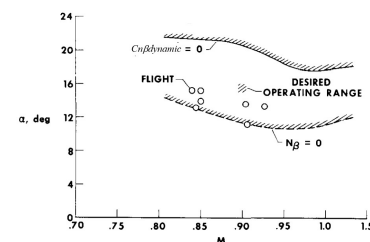Fig. 54 HL-10 wind tunnel data at M=2.16 [64]

Fig. 55 Flight Envelope Limitations of the X-24A [62]

Transforming this wind tunnel data onto a Weissman plot, see Fig. 56, we see that the airframe is firmly in region "F." Like the Bell X-2, the HL-10 does not achieve Skow's criteria ($C_{n\beta dynamic} > +0.004$) for strong resistance to spin departures. The aerodynamic properties also indicate that the Dutch-Roll will express itself as a strong wing rock; $\frac{\phi}{\beta} \cong 5$ at $\alpha = 12°$.

Layton [47] generalizes that lifting bodies lateral-directional handing is quite poor. He notes that unaugmented lifting bodies "are almost impossible to fly." He continues stating that if the airplane has both 1) effective ailerons **and** 2) favorable yaw, lateral-directional handling qualities can be solved with artificial roll damping. If the aircraft has large amounts of adverse yaw due to aileron deflection, it needs additional vertical fin area (i.e., strong positive static directional stability) to permit the implementation of an effective roll damper.

Flight test data of NASA's YF-12 noted $\zeta_{DR} \sim$ 0.8-radian/sec at subsonic speeds; $\omega_{DR} \sim$ 1.3 → 2.0 during the transonic and low supersonic and $\omega_{DR} \sim$ 1.00 → 1.36-radian/sec at $M \sim$ 3 cruise speeds. [54] With the *SAS* engaged, $\zeta_{DR} \sim$ 0.4 → 0.6 in the transonic and low supersonic and $\zeta_{DR} \sim$ 0.4 at $M \sim$ 3 cruise. [54] These frequencies and closed loop damping ratios are well within the *LEVEL 1* region of MIL-STD-8785C.

With its long service record, the YF-12 / SR-71 clearly demonstrated acceptable lateral-directional flying qualities at high speed. McMaster & Schenk note that the YF-12 "encounters low directional stability at high Mach numbers … [which] dictate full-time use of the yaw … stability augmentation systems (SAS) to provide … directional static stability." [65] Moes & Iliff extracted lateral-directional static stability derivatives for NASA's later SR-71 from flight test; see Fig. 57. [43] Considering *Izz/Ixx* ~ 5.3 and a typical supersonic cruise at $\alpha \sim$ 3°, we infer that $C_{n\beta dynamic} \sim +0.001$ which places it in Region "F" of the Weissman plot; incorporating *ARI* would likely lead it to more to favorable *LCDP*. The aerodynamic properties also indicate that the Dutch-Roll will express itself as a moderate wing rock; $\frac{\phi}{\beta} \cong 2.5$ at $M \sim 3.0$.

The XB-70 features more nuanced behaviors due to its scheduled wing-tip droop that reduced Mach effects in longitudinal aerodynamic stability; recall Fig. 29. Turning to Fig. 58, we see the increase in static directional stability due to the 65° drooped wingtips that also enable compression lift. Even with the drooped tips providing additional side facing projected area aft of the *CG*, we see that *dCn/dβ* declines from ~+0.1 per radian (+0.0017/°) at $M \sim$ 1.6 to ~+0.03 per radian (<+0.001/°) at $M \sim$ 3. The more troubling byproduct of the wingtip droop is the complete loss of effective dihedral at high supersonic speeds; *dCl/dβ* ~ +0.01 per radian (+0.0002 per degree) represents aerodynamic "anhedral" that counteracts formation of a stable Dutch-Roll. The aerodynamic properties also indicate that the Dutch-Roll will express itself as a tail-wag; $\frac{\phi}{\beta} \cong 0$ at $M \sim 3$.
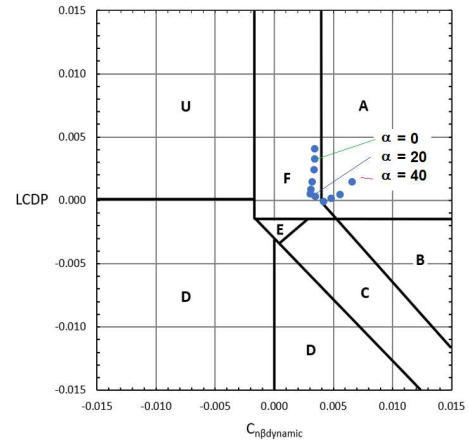

Fig. 56 Weissman Plot of the HL-10 derived from $M = 2.16$ wind tunnel data [64]
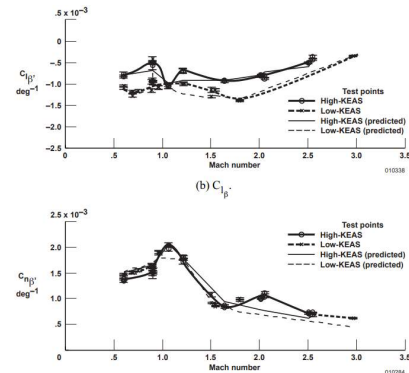

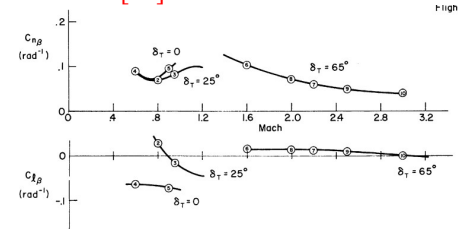Fig. 57 Lateral & Directional Stability of the YF-12 [43]

Fig. 58 Lateral & Directional Stability of the XB-70 [16]

Anderson [49] and White & Anderson [55] noted aileron adverse yaw issues during XB-70 flight test. Anderson states that "pilots commented that at supersonic speeds, the lateral-directional handling qualities are degraded by an adverse yaw experienced as a result of aileron deflection." [49] The adverse yaw is "approximately zero at low speed, highly adverse transonically [but] approach zero again at speeds above Mach 2;" [55] see Fig. 59. Thus, given its body heavy nature, we find that the XB-70 is clearly in Region "F" of the Weissman chart at all supersonic flight test conditions; see Fig. 60. While the static directional stability is strongest around $M \sim 1.6$ that flight condition coincides with the most unfavorable "anhedral" effect and worst adverse aileron yaw conditions.

The XB-70 flight test program revealed marginal lateral-directional flying qualities. Wolowicz & Yancey [39] note that "sideslip maneuvers … were adversely affected by a drop in static directional stability … at sideslip angles greater than ~2° for all Mach numbers and all wingtip configurations." White & Anderson [55] also note that the "aileron becomes a sideslipping control rather than a rolling control." When the pilot applies aileron to "stop a wing from dropping, sideslip is introduced, and the dihedral effect causes the airplane to tend to roll more and additional aileron is required." They state that an inattentive pilot is likely to "reach high sideslip angles inadvertently, especially, when flying in turbulence." Recall that MIL 8785C desires $\beta < \pm 0.17°$; so the fact that the XB-70 experienced such large sideslip excursions in flight is worrisome. Response to turbulence is experienced "primarily in roll, with less disturbance in pitch or yaw." Wolowicz & Yancey note that lateral-directional "maneuvers flown with the augmentation system off were [so] erratic [that they] usually could not be analyzed." [39]

In order to reenter, the Orbiter needs to fly its initial aerodynamic reentry at high angle-of-attack ($\alpha \sim 40°$) before reverting to basic gliding flight from M~5 to touchdown; see Fig. 61. [66] As with other slender vehicles, it has relatively high dihedral effect ($dCl/d\beta << 0$) which only grows with increasing α. The shuttle is quite "wing heavy;" $Izz/Ixx \sim 8$. Despite the visually large vertical tail, which becomes an effective "wedge" when the speed-brake split rudder is opened fully, the Orbiter lacks static directional stability. Nonetheless, due to its mass properties and nose-up flight attitude, the Orbiter demonstrates inherent Dutch-Roll stability throughout its entire reentry profile. The dominant contributor to $C_{n\beta dynamic}$ arises from the effective dihedral, not from the static directional stability.

None of the examined reports from the Space Shuttle program explicitly discuss stick-fixed Dutch-Roll frequencies or damping ratio.

Like so many other high-speed vehicles, the Orbiter exhibits strong adverse yaw from its ailerons. [66] Fig. 62 shows how the rolling moment from differential aileron holds across the entire reentry profile but how they develop substantial (30% to 50%)
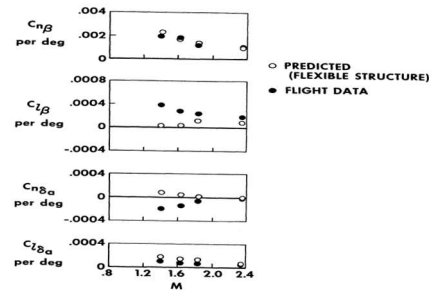

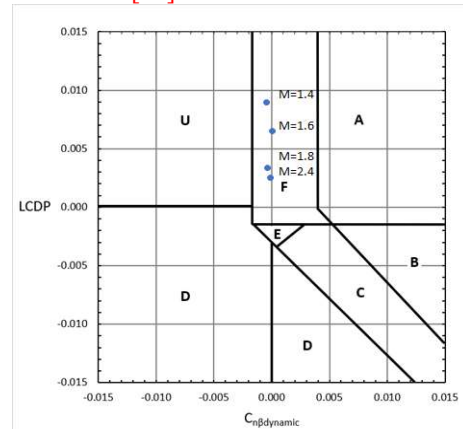Fig. 59 Lateral & Directional Stability of the XB-70 [49]

Fig. 60 Weissman Plot of the XB-70 from flight test data. $M = 1.4 \rightarrow 2.4$. Based on data from Ref. [49]
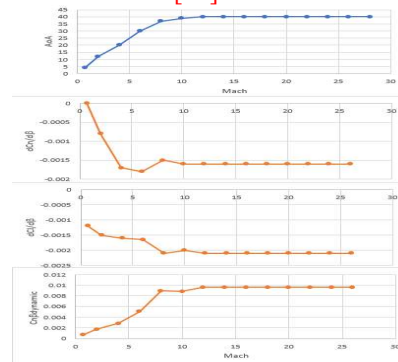

Fig. 61 Lateral, Directional & Dutch-Roll Stability of the Shuttle Orbiter from Flight Test Data. After Ref. [66]
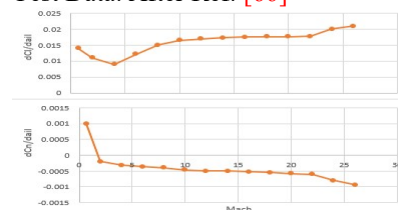

Fig. 62 Adverse Yaw of Shuttle Orbiter Ailerons from flight test data; moments per degree control surface deflection. Based on data from Ref. [66]

adverse yaw at all supersonic speeds. With the rudder dedicated to "speed-brake," in other words forming a symmetric wedge at speeds above Mach 2.5 (see Fig. 63), just like the X-2, the Orbiter has dangerous innate aerodynamic qualities if all lateral-directional control were to rely on the ailerons.

The Orbiter features a complex, "fly-by-wire" control system to handle the adverse yaw. As seen in the data presented in Figs. 64 and 65 if the Orbiter were reliant on just the aerodynamics of the ailerons it would have unacceptable control characteristics. At typical hypersonic speeds, 30° of aileron deflection would develop enough adverse yaw to force 10° of sideslip; far beyond the linear limit. The Weissman plot built upon the basic aerodynamic data, shows poor departure resistance if the pilot were reliant solely on aerodynamic control.

According to Gamble [69] the Orbiter was conceptualized to fly high cross-range reentry using "an all aerodynamic control concept." As aerodynamic data became available, it became clear that $LCDP$ was unfavorable. For a period of time, the Orbiter development team devised a curious strategy employing "reverse aileron control (negative aileron for positive roll)" for entry control. [69] Since this approach lacked robustness, the flight control system was revised to utilize "the yaw RCS jets to initiate bank maneuver and the ailerons to coordinate the maneuvers prior to activation of the rudder." [69] The RCS jets (recall Fig. 42) are used during reentry beginning at the very highest Mach numbers and lowest dynamic pressure. The "side-firing jets are used for directional control down to Mach 1.0, at which time the rudder becomes fully effective for directional control." [67] This combination of RCS and ARI functionally elevates $LCDP$ so that it has more favorable departure resistance according to the Weissman criteria. Because the RCS operates using pulse-width-modulation control of discrete hydrazine thrusters, it is difficult to come up with a precise numerical value of augmented $LCDP$.

Gamble [69] reiterates that "$LCDP$ was the first controllability criterion that was systematically applied to the Orbiter" followed by $C_{n\beta dynamic}$. RCS jet activation is governed by a flight control feedback loop that senses side accelerations; however, the jets are not strong enough to synthesize true directional stability. Since the fully functioning RCS system can only increase $C_{n\beta dynamic}$ by
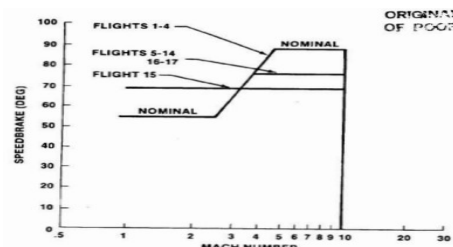

Fig. 63 Split Rudder "Speed-Brake" Schedule for Orbiter Reentry. [68]
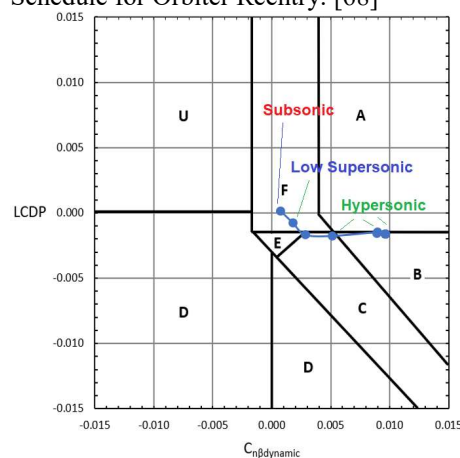
Fig. 64 Weissman Plot of the Shuttle Orbiter reentry profile flight test data. Unaugmented aileron-only control; no ARI; no RCS. Based on data from Ref. [66]
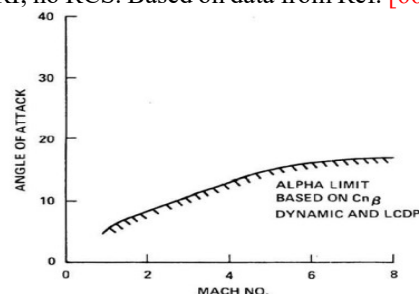
Fig. 65 Minimum Angle-of-Attack Limit for Shuttle Orbiter [69]

+0.002, the Orbiter is restricted to flight above a critical angle-of-attack where the dihedral effect still dominates the Dutch-Roll stability (see Fig. 65). This is an unusual schedule in light of earlier experience with the X-24A where operations were restricted to flight below a critical angle-of-attack; recall Fig. 55. However, both schedules derive from the same principles: a controllable aircraft needs to display non-divergent lateral-directional modes and an ability to command roll without excessive sideslip.

Of the more recent high-speed vehicles with proprietary data, we can only note generalities. Neither X-43A nor X-51A were advertised as being maneuvering airframes. Both flight test programs were marred by launch failures, but ended with a successful run of their respective scramjet engines over their intended trajectories.

Circumstantial evidence from the failure of the first launch of the HTV-2 indicates lateral-directional controllability deficiencies. The ostensible goal of the HTV-2 was to "develop and test an unmanned, rocket-launched, maneuverable, hypersonic air vehicle that glides through the Earth's atmosphere up to Mach 20 speed." [70] After launch from a Minotaur IV booster, the HTV-2 experienced "flight dynamics anomalies" and departed controlled

flight during a "pull-up maneuver." [70]   The independent engineering review board identified "higher than predicted adverse yaw coupled into roll that exceeded the available roll control capability" as the proximate cause of the crash. [70] Referring to Fig. 66, the board describes a departure consistent with that experienced by the X-2. In the presence of a roll disturbance, the flight control system differentially deflected its body flaps to arrest a developing roll rate. The interplay between adverse yaw from the "aileron" and the dihedral effect leads to a sideslip "run-away" and control power saturation. The remediation plan was to alter the flight profile to fly at a lower angle-of-attack, adjust the vehicle CG, and augment aerodynamic controls with RCS. After following these recommendations, Lockheed's second HTV-2 test flight was more successful. [70]

D. Bandwidth and Frequency Coupling Concerns

The inherent longitudinal dynamics of an airframe must be well matched to maneuvering expectations so that the airframe follows command inputs without excessive phase lag. If airframe response sufficiently trails command inputs, the airframe may inadvertently oscillate. If a classical design follows MIL-STD-8785C Control Anticipation Parameters, it should be resistant to pilot-induced-oscillations during normal operations. [19]

As discussed in Section IV.G, dynamic mode coupling issues can arise when the Short-Period and Dutch-Roll frequencies lie too close to one another.

Beginning with the X-2 and Fig. 67, we consider how the Short-Period and Dutch-Roll frequencies interact as the aircraft flies its full, planned final mission. Both Short-Period and Dutch-Roll frequencies are strong functions of dynamic pressure and moderate functions of Mach number. The Dutch-Roll, alone, is also strongly dependent upon angle-of-attack. Both frequencies slow for approach and landing as well as during the "over-the-top" ballistic portion of flight above 65,000-ft. Although the pilot lost control at the beginning of the "pull-up" maneuver at Mach 3+ and 70,000-ft, neither the Short-Period nor Dutch-Roll frequency taken in isolation was the cause of the crash. Taken together, we see that frequencies do cross on numerous occasions: 1) during initial powered ascent around 45,000-ft, 2) at the beginning of the ballistic "over-the-top" maneuver and 3) just at the beginning of the "pull-up" maneuver – just where control was lost. Thus, inertia-coupling where lightly damped (due to high speed and altitude) modes cross-talk was a contributory factor to the crash. The coupling between Short-Period and Dutch-Roll Modes explains a source of lateral-directional energy that led to the high slideslip angles associated with adverse-yaw which precipitated loss-of-control. [51]

Turning next to the X-15, we see that it is also prone to Inertial Coupling. We can see that the frequencies are generally distinct, and only get close to one-another while "going over the top;" see Fig. 68. Since Inertial Coupling is likely to occur only as the X-15 flies
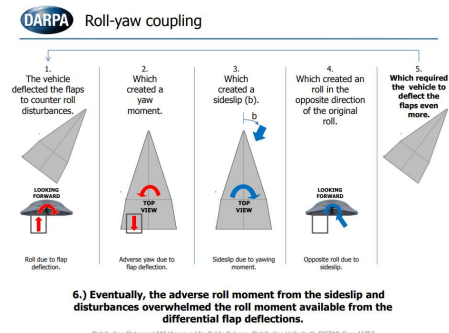

Fig. 66 Summary of Lockheed HTV-2 test flight #1 departure from controlled flight [70]
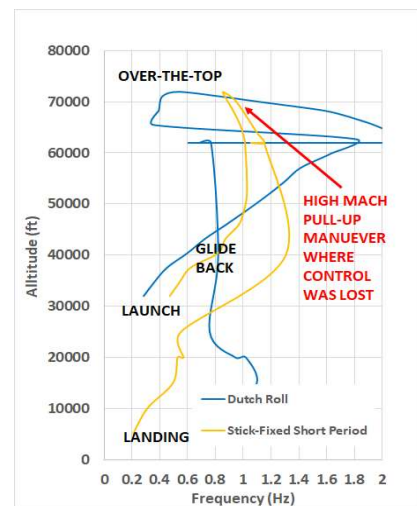

Fig. 67 X-2 Short-Period and Dutch-Roll Frequency Estimates over a High-Mach / High-Altitude Flight [51]
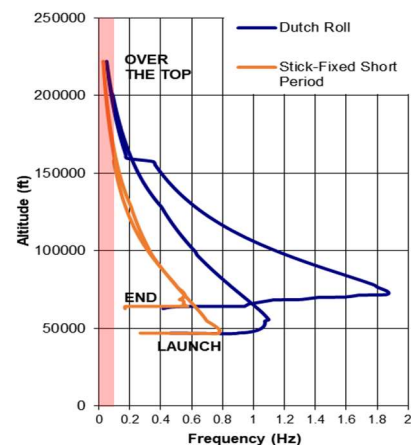

Fig. 68 X-15 Short-Period and Dutch-Roll Frequency Estimates for an Atmospheric Reentry Flight Profile [12]

"over the top," where the rigid-body frequencies are already so low as to need supplemental control from reaction-control, this flight does not raise concern. [12]

Among the lifting bodies, the X-24A did not appear to suffer from inertia-coupling as reported longitudinal Short-Period frequencies did not coincide with Dutch-Roll frequencies. [42] Hoey noted that "in the transonic and supersonic flight regime, the roll response did not meet the specification requirements with *SAS* on." [42] The roll time constant, τ_R, was found to be as much as 50% longer than the *LEVEL 3* minimum (2-sec to 45°) in the transonic; but exceeded *LEVEL 1* requirements (1.2-sec to 45°) during approach-and-landing. That said, poor pilot reviews resulted from pilot-induced-oscillation (PIO) sensitivity rather than low roll power. [42] At odds with MIL-STD-8785C specification compliance, pilots felt that "the rolling capability was adequate for all phases of the X-24A mission, except for landing in a crosswind or [flight in] moderate turbulence." [42]

While Hoey did not mention Inertia Coupling, he did mention that the X-24A had a Lateral-Phugoid frequency coupling between the long-period Roll and Spiral-Modes. [42] "All SAS-off conditions exhibited an oscillatory, coupled Roll-Spiral-Mode" which is impermissible under MIL-STD-8785C. [19] Given the >20-sec time constant of this mode, it was "never observed in flight … although test maneuvers confirmed values of the derivatives that contributed to [it.]" [42] Hoey continues stating that under normal *SAS* gain settings, the Lateral-Phugoid divided into distinct non-oscillatory roll and Spiral-Modes; these gains "were chosen so as to avoid the coupled Roll-Spiral-Mode whenever possible." [42]

The HL-10 likely had troubling inherent inertia coupling based on its mass properties, $\left|\frac{Ixx - Iyy}{Izz}\right| \sim 0.7$ as, well as closely spaced Short-Period and Dutch-Roll frequencies; both being around 4→5 radian/sec. [72] With its weak dihedral effect, the HL-10 probably did not suffer from Lateral-Phugoid issues. Pilot comments, flying the revised *SAS* programming, did not mention any sorts of handling qualities degradation due to inertia coupling or Lateral-Phugoid. [72]

On NASA's YF-12, pilot reports did not mention inertia coupling. [54] Flight test revealed that the roll time constant was as short as $\tau_R = 0.27$-sec during approach and landing, and typically $\tau_R = \sim 1.2$-sec at Mach 3+ high altitude cruise. Thus, roll responsiveness achieve *LEVEL 1* capabilities across much of the flight envelope. [54] The spiral stability was positive and was "well within the military specification requirement of a time to double of no less than 20-seconds." [54] Thus, the YF-12 / SR-71 family seems immune from Lateral-Phugoid issues.

Bourne & Kirsten [71] note that earlier versions of the Orbiter flight control system were prone to PIO during final approach and touchdown; the primary causes for this behavior were "inadequate pitch attitude visual reference cues" (poor cockpit visibility with the nose high final approach) and poor pitch responsiveness. Pilot bandwidth and phase response had to accommodate a "one-half-second delay … between pitch stick command input and normal acceleration response partly due to the digital control system and partly due to vehicle geometry." [71] We note that a 0.5-sec group delay introduces a minimum of ~45° phase lag on a 4-sec period; 1.6-radian/sec. Since Orbiter aerodynamic data (subsonic $dCL/d\alpha \sim +0.048$/deg, and 200-KEAS final approach flown at $W/S \sim 70$ lbm/ft^2) indicates that $n/\alpha \sim 5$, our interpretation of MIL-STD-8785C standards would suggest a desired longitudinal bandwidth $> \sim 0.9$-radian/sec (a 7-sec period). Thus, we concur that the Orbiter had sufficient bandwidth to fly approach and landing but was PIO prone due to control system group-delay. Indeed, to resolve the PIO issues prior to STS-1, NASA added a PIO suppression filter into the pitch controller that "reduced pilot command inputs as a function of pitch command frequency." [71] The Orbiter is a good example of how a "fly-by-wire" system can reduce the spectral content of control command to avoid phase issues associated with fundamental modes.

VI. Summary and Conclusions

This review paper collects many stability and control screening metrics suitable for high-speed airframe design together in one place. These metrics, which are a subset of methods found in MIL-STD-8785C, MIL 1797B and older AGARD reports, evaluate novel candidate configurations for stability and control deficiencies. Many of these metrics stem from "lessons learned" on prior military aircraft programs; others derive from the development of the Space Shuttle Orbiter. We demonstrate the broad utility of these metrics by post-processing old wind tunnel and flight-test data to show how flight success and failure can be predicted from data now available to the modern design team early in the design process.

A low-risk future high-speed vehicle should be engineered to be statically stable in pitch ($dCm/d\alpha$ < 0) with a stick-fixed frequencies compliant with control anticipation parameter charts found in MIL-STD-8785C and MIL-STD-1797B; refer back to Fig. 15. If the engineering team decides upon a configuration where $dCm/d\alpha$ > 0, the closed-loop control system needs to demonstrate adequate gain and phase margin to follow minimum longitudinal bandwidth requirements derived from MIL-STD-8785C and MIL-STD-1797B; refer back to TABLE 3.

A low-risk high-speed vehicle should be engineered to achieve static pitch trim across their intended flight (M, α) and mass properties (CG) envelope with <75% of maximum theoretical control power. If substantial synthetic stability or damping is needed, the static control power requirement may need to be made more conservative yet; i.e. static trim with <60% of maximum theoretical control power.

Since high-speed vehicles are inherently slender, they are prone to inertia coupling and control-coupling; synthetic pitch damping is essential.

A low-risk high-speed vehicle should inherently present a stable Dutch-Roll Mode, $C_{n\beta dynamic}$ > 0. Lateral-directional rigid-body modes (Dutch Roll, Spiral and Roll) should follow guidelines found in MIL-STD-8785C. Since high-speed vehicles have substantial adverse yaw from roll control, significant static directional stability ($dCn/d\beta$ >> 0) is desired to ensure that full "aileron" deflection (considering control allocation such as ARI) does not drive the vehicle to significant sideslip angles. The handling qualities of the early X-15, the XB-70 and the lifting body configurations (X-24A and HL-10) were degraded because a significant proportion of their directional stabilizing surfaces were ventrally mounted; a vehicle with effective aerodynamic dihedral, $dCl/d\beta$ < 0, stemming from a dorsal vertical stabilizer presents reduced flight risk.

The Bihrle-Weissman chart ($C_{n\beta dynamic}$ vs $LCDP$) is an effective screening tool. Low-risk vehicles present in the "A" region of the chart. Vehicles which inhabit the "F" region often exhibit performance degrading handling qualities limitations. A lack of attention to Bihrle-Weissman type criteria and lateral-directional control-coupling lead to operational loss of control of the X-2 and HTV-2. Supplemental RCS can mitigate these issues under limited flight conditions. While successful flights of the Space Shuttle Orbiter and HTV-2 testify to this possibility, an active RCS system adds weight and complexity. If the RCS propellant load is expended, such a vehicle will depart from controlled flight.

Synthetic lateral-directional damping is essential since aerodynamic damping declines with increasing flight speed.

The Lateral-Phugoid mode is possible on any slender vehicle that exhibits strong dihedral effect and weak roll damping. The $\frac{\phi}{\beta}$ ratio determines if a roll damper or yaw damper will prove most effective. Configurations should be screened to ensure that their Short-Period and Dutch-Roll frequencies do not overlap (inertia coupling), and that Roll-Mode and Spiral-Mode time constants do not overlap (Lateral-Phugoid divergence); if they do, the FCS needs to suppress these modes.

Unlike a technology demonstrator, whose flight profile may be tightly constrained, general purpose high-supersonic and hypersonic aircraft need to operate over a wide range of flight conditions and mass properties. An unpiloted vehicle, engineered to conform to select piloted handling qualities metrics, reduces risks that can jeopardize program success. In all cases, engineering needs to identify the necessary longitudinal and lateral-directional bandwidth requirements as early as possible in the design process.

Engineers can utilize all of these metrics using widely available aerodynamic data. At the conceptual, trade-study level, empirical and rapid-computational tools (vortex-lattice, Newtonian and other panel methods) can be used to rapidly develop databases. At preliminary design, a cocktail of methods introducing limited amounts of volume-grid CFD and wind tunnel data can augment the conceptual aerodynamic database. For detail design, the Space Shuttle Orbiter program can serve as an excellent role model; the Orbiter engineering team applied these screening techniques to a multi-fidelity database with an associated uncertainty model.

Acknowledgements

References

1. Arrington, J.P. and Jones, J.J., ed., "Shuttle Performance: Lessons Learned," NASA CP 2283 Part 1, 1983.
2. "Proceedings of the X-15 First Flight 30th Anniversary Celebration." NASA CP-3105, 1989.
3. Jenkins, D.R. and Landis, T.R., Hypersonic: The Story of the North American X-15, Specialty Press, North Branch, MN, 2003.
4. Chudoba, B., Stability and Control of Conventional and Unconventional Aerospace Vehicle Configurations, Springer, Switzerland, 2019.
5. Coleman, C.C. and Farqui, F.A., "On Stability and Control of Hypersonic Vehicles," Australian Defence Science & Technology Office Report, DSTO TR-2358, 2009.
6. Larson, G.L., Klyde, D.H., Myers, T.T., McRuer, D.T.and Suchomel, C., "Military Missions And Linearized Model For A Hypersonic Vehicle," AIAA 95-0851, 1995.
7. Day, R.E., "Coupling Dynamics in Aircraft Design: A Historical Perspective," NASA SP-532, NASA, 1997.
8. *See:* https://www.af.mil/About-Us/Fact-Sheets/Display/Article/104557/aim-9-sidewinder/
9. *See:* https://www.af.mil/About-Us/Fact-Sheets/Display/Article/104467/x-51a-waverider/
10. Weill, J., "Review of the X-15 Program," NASA TN D-1278, 1962.
11. Romere, P.O. and Whitnah, A.M., "Space Shuttle Entry Longitudinal Aerodynamic Comparisons of Flights 1-4 With Preflight Predictions," NASA CP 2283 Part 1, 1983.
12. Griffin, J.A. and Takahashi, T.T., "Aero-Spaceplane Mission Performance Estimations Incorporating Atmospheric Control Limits," AIAA 2022-3656, 2022.
13. Smith, A.M.O., "High Lift Aerodynamics," AIAA J. Aircraft Vol 12, No. 6, pp. 501-530, 1975.
14. Ladson, C.L., "Effects of independent variation of Mach and Reynolds numbers on the low-speed aerodynamic characteristics of the NACA 0012 airfoil section," NASA TM-4074, 1988.
15. Bertin, J.J., Hypersonic Aerothermodynamics, AIAA, 1993.
16. Heffley, R.K. and Jewell, W.F., "Aircraft Handling Qualities Data," NASA CR-2144, 1972.
17. McLellan, C.H., "A Method for Increasing the Effectiveness of Stabilizing Surfaces at High Supersonic Mach Numbers," NASA RM L54F21, 1954.
18. Takahashi, T.T., Aircraft Performance and Sizing, Volume II: Applied Aerodynamic Design, Momentum Press, New York, 2016.
19. MIL-F-8785C, Military Specification: Flying Qualities of Piloted Airplanes, 1980.
20. Koven, W. and Wasico, R., "Flying Quality Requirements for United States Navy and Air Force Aircraft," AGARD 336, 1961.
21. Yechout, T.R., Introduction to Aircraft Flight Mechanics, Second Edition, AIAA, 2014.
22. Roskam, J., Airplane Flight Dynamics and Automatic Flight Controls, Pt. I., DAR Corporation, 1995.
23. Roskam, J., Airplane Flight Dynamics and Automatic Flight Controls, Pt. II., DAR Corporation, 1995.
24. Rudd, L.v.E., Hodgkinson, J., Parker, R., Tarpley,C., "Hypersonic Stability Derivative Modeling Issues," AIAA 2010-7929, 2010.
25. Stich, R., Sachs, G. and Cox, T., "New Longitudinal Handling Qualities Criterion for Unstable Hypersonic Vehicles," AIAA 2003-5309, 2003.
26. Seltzer, R.M. and Rhodeside, G.R., "Fundamentals and Methods of High-Angle-of-Attack Flying Qualities Research," NADC-88020-60, AD-A235-994, 1988.
27. Skow, A.M. and Titiriga, A., "A Survey of Analytical and Experimental Techniques to Predict Aircraft Dynamic Characteristics at High Angles of Attack," AGARD CP-235, 1978.
28. MIL-STD-1797A, Flying Qualities of Piloted Aircraft, 1995.
29. MIL-STD-1797B, Flying Qualities of Piloted Aircraft, 2006.

30. Mitchell, D.G., Klyde, D.H., Pitoniak, S., Schulze, P.C., Manriquez, J.A., Hoffler, K.D. and Jackson, E.B., "NASA's Flying Qualities Research Contributions to MIL-STD-1797C," NASA CR-2020-5002350, 2020.
31. Weissman, R., "Status of Design Criteria for Predicting Departure Characteristics and Spin Susceptibility," AIAA 74-791, 1974.
32. Weissman. R., "Preliminary Criteria for Predicting Departure Characteristics' Spin Susceptibility of Fighter-Type Aircraft," AIAA Journal of Aircraft, Vol. 10, No. 4, April 1973.
33. Johnston, D.E., Mitchell, D.G. and Myers, T.T., "Investigation of High Angle-of-attack Maneuver Limiting Factors," AFWAL-TR-80-3141, 1980.
34. Carter, C.V., "A Discussion of Theoretical Methods for Prediction of Spin Characteristics," Proceedings of the WADC Airplane Spin Symposium, 57 WCLC-1688, 1957, pp. 195-201.
35. Kalviste, J., "Aircraft Stability Characteristics at High Angles-of-Attack. Dynamic Stability Parameters, AGARD CP 235, May 1978.
36. Mason, W.H., "High Angle-of-attack Aerodynamics" see: http://www.dept.aoe.vt.edu/~mason/Mason/AeroHighAlpha.html
37. Philips, W.H., "Effect of Steady Rolling on Longitudinal and Directional Stability," NACA TN-1627, 1948.
38. Cotting, M.C., Personal Communication, 2022.
39. Teodorescu, B.C., "Lateral Directional Oscillatory Departure Criteria for High Angle-of-attack Flight Conditions," U.P.B. Sci. Bull., Series D, Vol. 68, No. 3, 2006.
40. Day, R. and Reisert, D., "Flight Behavior of the X-2 Research Airplane to a Mach Number of 3.20 and a Geometric Altitude of 126,200 Feet," NASA TM X-137, 1959.
41. Holleman, E.C. and Reisert, D., "Controllability of the X-15 Research Airplane with Interim Engines During High-Altitude Flight," NASA TM X-51A4, 1961.
42. Hoey, R.G., "Flight Test Handling Qualities of the X-24A Lifting Body," AFFTC TD-71-11, 1971.
43. Moes, T. and Iliff, K., "Stability and Control Estimation Flight Test Results for the SR-71 Aircraft With Externally Mounted Experiments," NASA/TP 2002-210718, 2002.
44. Wolowicz, C.H., Strutz, L.W., Gilyard, G. and Matheny, N.W., "Preliminary Flight Evaluation of the Stability and Control Derivatives and Dynamic Characteristics of the Unaugmented XB-70-1 Airplane Including Comparisons with Predictions," NASA TN D-4578, 1968.
45. Scheiss, J.R., "Lateral Stability and Control Derivatives Extracted from Space Shuttle Challenger Flight Data," N88-16788, NASA TM 100520, January 1988.
46. Wolowicz, C. H. and Yancey, R.B., "Summary of Stability and Control Characteristics of the XB-70 Airplane," NASA TM X-2933, 1973.
47. Layton, G. P. Jr., "Interim Results of the Lifting-Body Flight Test Program," NASA TM X-1827, 1969.
48. Kirsten, P.W., Richardson, D.F. and Wilson, C.M., "Predicted and Flight Test Results of the Performance, Stability and Control of the Space Shuttle from Reentry to Landing," NASA CP-2283 Vol. I, 1983.
49. Andrews, W.H., "Summary of Preliminary Data Derived from the XB-70 Airplanes," NASA TM X-1240, 1966.
50. Suit, W.T. and Scheiss, J.R., "Lateral and Longitudinal Stability and Control Parameters for the Space Shuttle Discovery as Determined from Flight Test Data," NASA TM 100555, 1988.
51. O'Brien, K.P. and Takahashi, T.T., "An Investigation of the Bell X-2 and the Factors that Led to Its Fatal Accident," AIAA 2022-3203, 2022.
52. Banner, R.D., Kuhl, A.E. and Quinn, R.D., "Preliminary Results of Aerodynamic Heating Studies on the X-15 Airplane," NASA TM X-638, 1962.
53. Kempel, R.W., Painter, W.D. and Thompson, M.D., "Developing and Flight Testing the HL-10 Lifting Body: A Precursor to the Space Shuttle," NASA RP-1332, 1994.
54. Berry, D.T., Mallick, D.L. and Gilyard, G.B., "Handling qualities aspects of NASA YF-12 flight experience," Proceedings of the SCAR Conference, Vol. I, 1976.
55. White, A.S. and Anderson, P.H., "Operational Experience at Mach 3," AGARD CP-17, 1966.
56. "Open Discussion" AGARD CP-106, 1971.
57. Bailey, A.J., Jr., "Development & Flight Test of Adaptive Controls for the X-15," Honeywell Contractor Report 412TW-PA-22050, 412th Test Wing, Edwards AFB, CA.
58. Dehney, C.J., Orr, J.S., Barshi, I. and Statler, I.C., "A Analysis of the X-15 Flight 3-65 Accident," NASA/TM-2014-218538, 2014.
59. Gamble, J., "The Application of Aerodynamic Uncertainties in the Design of the Entry Trajectory and Flight Control System of the Space Shuttle Orbiter," NASA CP 2283 Part 1, 1983.
60. Hardy, G.H., "Space Shuttle Orbiter Handling Quality Criteria Applicable to Terminal Area, Approach and Landing," Space Shuttle Aerothermodynamic Technical Conference, Vol. 4, 1972.

61. Armstrong, J.G., "Flight Planning and Conduct of the X-15A-2 Envelope Expansion Program," AFFTC TD-69-4, 1969.

62. Peterson, F.S., Rediess, H.A. and Weil, J., "Lateral Directional Control Characteristics of the X-15 Airplane," NASA TM X-726, 1962.

63. Manke, J.A. and Retelle, J.P., "Assessment of Lifting Body Vehicle Handling Qualities," AIAA 71-310, 1971.

64. Campbell, J.F. and Watson, C.B., "Stability and Control, Hinge Moment and Pressure Coefficient Data for the HL-10 Manned Lifting Entry Vehicle at Mach Numbers from 1.41 to 2.16," NASA TM X-1300, 1966.

65. McMaster, J.R. and Schenk, F.L., "Development of the F-12 Aircraft Flight Control System," J. Aircraft Vol. 11, No. 4, April 1974, pp. 225.

66. Compton, H.R., Schiess, J.R., Suit, W.T, Scallion, W.I. and Hudgins, J.W., "Stability and Control Over the Supersonic and Hypersonic Speed Range," NASA CP 2283 Part I, 1983.

67. Stone, J.S., Baumbach, J.J. and Roberts, B.B., "Space Shuttle Orbiter Reaction Control Subsystem Flight Data Anomalies," NASA CP 2283 Part I, 1983.

68. Cooke, D.R., "Minimum Testing of the Space Shuttle Orbiter for Stability and Control Derivatives," NASA CP 2283 Part I, 1983.

69. Gamble, J., "The Application of Aerodynamic Uncertainties in the Design of the Entry Trajectory and Flight Control System of the Space Shuttle Orbiter," NASA CP 2283 Part I, 1983.

70. Schulz, C. and Wetherall, R., "Falcon Hypersonic Technology Vehicle (HTV-2) Industry Team Expo Briefing," DISTAR Case 16757, May 24, 2011.

71. Bourne, C.A. and Kirsten, P.W., "Approach and Landing Characteristics of the Space Shuttle Orbiter," NASA CP 2283 Part I, 1983.

72. Kempel, R.W. and Manke, J.A., "Flight Evaluation of HL-10 Lifting Body Handling Qualities at Mach Numbers from 0.30 to 1.86," NASA TN D-7537, 1974.